INFORMATION TO USERS

8008665

WARBURTON, JOHN DUTTON

THE USE OF THE FINITE-ELEMENT METHOD IN METEOROLOGICAL MODELLING

The University of Oklahoma   PH.D.   1979

University
Microfilms
International 300 N. Zeeb Road, Ann Arbor, MI 48106   18 Bedford Row, London WC1R 4EJ, England

THE UNIVERSITY OF OKLAHOMA

GRADUATE COLLEGE

THE USE OF THE FINITE ELEMENT METHOD

IN METEOROLOGICAL MODELLING

A DISSERTATION

SUBMITTED TO THE GRADUATE FACULTY

in partial fulfillment of the requirements for the

degree of

DOCTOR OF PHILOSOPHY

By

JOHN DUTTON WARBURTON

Norman, Oklahoma

1979

DEDICATION

To Anne, my strength

ACKNOWLEDGMENTS

ABSTRACT

The finite element method may relieve some of the
problems associated with numerical modelling of the atmos-
phere. The method reduces the problem of nonlinear computa-
tional instability, allows arbitrary placement of grid points,
and offers greater flexibility in the handling of boundary
conditions. In addition, the finite element method has been
shown to be more accurate for some types of problems.

This research concentrates on the ability of the
finite element method to serve as the means of solving the
equations which describe flow in the atmosphere and provides
answers as to the type of finite element approximation best
suited for meteorological research. Five different finite
elements using both linear and quadratic interpolation are
tested in the space domain. Several time differencing schemes
are also tested with the elements in order to determine the
most accurate and efficient configuration. In addition, the
concepts of lumped and consistent mass are examined and tested
as well as alternative methods of handling the computer im-
plementation of the method.

It is found that the finite element method using the
four-node bilinear rectangular element provides the most

accurate handling of the spatial derivatives. Combined with the Crank-Nicholson time difference scheme using consistent mass, the four-node element is not only the most accurate in the handling of advective flow but also controls the growth of gravity waves the longest. This study also shows that when explicit time difference schemes such as the Leap-frog scheme are used with consistent mass the degradation in results when compared to the Crank-Nicholson method is minimal.

From the standpoint of computational efficiency, the finite element method is shown to be competitive with certain finite difference methods under certain special conditions. For constant grid spacing the finite element version of a simple vorticity-stream function model using the four-node bilinear element can be converted into an expression identical to the Arakawa Jacobian in space. However, unlike Arakawa's method, the finite element method includes consistent mass, a more accurate distribution of the mass than found in conventional finite difference methods which use the lumped mass concept. This special finite difference form of the finite element method requires slightly more computation but is more accurate than its finite difference counterpart.

It is evident that further study of the finite element method as an alternative to finite difference methods is warranted. Its use in the future may solve many existing problems in current atmospheric models as well as providing more accuracy in the solutions of the equations.

TABLE OF CONTENTS

LIST OF FIGURES

ix

LIST OF TABLES

LIST OF SYMBOLS

[A]	nonlinear advection matrix
c	wave speed
d	grid spacing
e	element (used as subscript or superscript)
f	Coriolis term
FDM	finite difference method
FEM	finite element method
g	gravitational acceleration
h	height of free surface of fluid in shallow water equations
i,j	used as subscripts to denote a grid point
[J]	nonlinear Jacobian matrix
J(p,q)	Jacobian operator
[M]	mass matrix
n	used as a superscript to denote the discrete time
N_i	finite element interpolation (shape) functions
n_x, n_y	components of unit normal vector in x and y directions
p	pressure
t	time
t_x, t_y	tractions in x and y directions
u	component of velocity in x direction
v	component of velocity in y direction
β	a constant, given by rate of change of Coriolis parameter with respect to latitude (y)
Δ	used to denote a change (e.g. Δt implies time change)

ψ stream function

ρ_o constant density

θ used to denote time difference scheme (e.g. $\theta = 0.5$ denotes Crank-Nicholson)

Ω global domain of problem

$\partial\Omega$ boundary of Ω

ζ vorticity

∇^2 Laplacian operator

THE USE OF THE FINITE ELEMENT METHOD

IN METEOROLOGICAL MODELLING

CHAPTER I

INTRODUCTION

A large percentage of current meteorological research
involves the development of numerical models. The majority
of those models are designed using the finite difference
method (FDM) to represent the derivatives in the differential
equations. The use of the FDM in meteorological models leads
to difficulties in several areas. For example, many differ-
encing schemes result in damping of important waves, inaccur-
acies in phase speeds, or computational instability (Messinger
& Arakawa, 1976). In addition, finite difference methods are
not equipped to handle irregular boundaries. Finally, one of
the most difficult situations for the FDM is grid nesting, an
important feature in numerical forecasting which allows for
grid refinement in areas of interest so that smaller scale
features can be identified and predicted with greater accuracy.

One method which may relieve some of the problems of
finite differencing is the finite element method (FEM). The
FEM employs local interpolating functions over finite sub-

domains which are connected together to approximate the global system. The governing partial differential equations are expressed in integral form. Normally this is accomplished using the Galerkin method which allows for easy derivation of the integral form of complex systems of partial differential equations. Details on the Galerkin method are given in Appendix A.

Because integral equations are solved, the FEM satisfies important global conservation laws associated with the model equations, regardless of the shape of the domain. Thus, computational instability is much less of a problem. The nodal (grid) points may be placed arbitrarily so that fine resolution can be used in an area of interest, with coarse resolution in areas of weak gradients. Higher order approximations are easily used without special boundary conditions. There is greater flexibility in the handling of boundary conditions. Finally, the FEM has been shown to be more accurate than the finite difference method for some types of problems.

In summary, the finite element method and finite difference method are fundamentally different. Finite difference equations are derived from truncated Taylor Series expansions. The assumption is that these approximations offer sufficient accuracy for the representation of differential equations which govern physical processes. In some finite difference methods, the concentration is on the partial differential equation and the approximation of derivatives at

2

a point. The finite element method is global in nature; it is a variational method which uses integral equations.

This research concentrates on the ability of the FEM to serve as the means for solving the equations which describe flow in the atmosphere and provides answers as to the type of finite element approximation best suited for meteorological research. The FEM is examined in several different ways in order to determine the more accurate and cost-effective ways in which it can be employed. Five different elements using both linear and quadratic interpolation are tested in the space domain. These elements and interpolation functions are discussed in Appendix A. Several time differencing schemes are tested with the elements in order to determine the most accurate and efficient configuration. In addition, the effect of using consistent versus lumped mass is tested. This difference is concerned with the handling of the time derivative. When lumped mass is used, the mass of an element is said to be equally distributed to the nodes (or mesh points). In contrast, consistent mass means that there is a weighted distribution of the mass. Lumped mass is analogous to the finite difference method and is a compromise which can be made in the FEM. Consistent mass naturally arises in the finite element formulation. This concept is discussed in detail in Chapter III.

The tests described above are performed using three different formulations for flow in a periodic channel. First

a vorticity-stream function formulation with known analytic solution is used for all the tests described above. Then the same type of flow is studied using the penalty method for comparison. In the penalty method the pressure terms are eliminated in the functional; however, the model allows for approximate pressure calculations. Only the tests involving element accuracy are repeated for the penalty model. Finally, the shallow water equations are used to study element accuracy, time differencing methods, and the conservative properties of the FEM.

Most of the published research on the FEM by meteorologists has involved a specific problem with the FEM applied in a specific manner. There has been no careful investigation as to what type of finite element approximation is best suited to meteorological problems. This research provides a strong foundation for further application of the FEM in advanced meteorological models. The results presented here show that it is feasible to apply the FEM to non-linear flow problems where advection is significant. A four-node quadrilateral element with linear interpolation provides the best results and the FEM is shown to be more accurate than the FDM.

Chapter II provides insight into the historical developments of the FEM, as well as the relationship of this work to published research. Chapter III gives the methodology including a discussion of the governing equations and numerical procedures. The results are presented in Chapter IV and

4

conclusions and remarks in Chapter V. There are appendices describing the finite element approximation in detail and the numerical stability for the four-node rectangle.

CHAPTER II

BACKGROUND

Historical Development

The variational approach to the solution of differ-
ential equations is the basis of such discoveries as Hamil-
ton's Principle on the mechanics of moving particles, the
Schrodinger wave equation, and contributed to Einstein's dev-
elopment of the theory of relativity (Simmons, 1972). The
variational method of solving differential equations is quite
elegant for certain special cases; however, its general appli-
cability has been delayed until modern times due to technical
problems. Approximate methods were introduced by Rayleigh
and Ritz during the late 1800's in which the variables were
expressed as a linear combination of some approximating func-
tions and the integral over the domain of the error was mini-
mized. The method received considerable attention but it is
difficult to apply for problems with irregular boundaries or
complex boundary conditions and cannot be used for nonlinear
problems.

A break occurred in the 1940's when Courant solved
the St. Vincent torsion problem by approximating the warping

6

function through a combination of linear triangles assembled over the domain and formulating the problem using the principle of minimum potential energy (Oden, 1972). It is found that if the elements are relatively small, the variation of functions within them can be adequately represented by a low-order polynomial. If certain continuity requirements were met along the element boundaries, complex systems could be reasonably solved.

The method came to the forefront in the 1960's when its use became widespread, particularly in areas such as airframe design. Since the advent of large scale computer systems, the use of the FEM has grown rapidly in several areas of engineering; however, it has only been in the 1970's that interest in the method has begun to develop among meteorolgists.

Current Literature

Other than the University of Oklahoma, School of
Meteorology, there are four main groups investigating the
application of the FEM to meteorological problems.

Naval Postgraduate School, Monterey, California

Meteorological Office, Bracknell, England

Atmospheric Environment Service, Quebec

Lawrence Livermore Laboratory, Livermore, California

Additionally, there has been some related research by civil
engineers and oceanographers such as Kawahara (1977 a, b, c),
Platzman (1978), and Fix (1975) who have employed the shallow
water equations. This survey of current literature will
provide a capsule description of the state of meteorological
FEM research and emphasize the need for this study.

Work at the Naval Postgraduate School culminated with
the publication of Kelly and Williams (1976) which was a study
of barotropic flow in a periodic channel. The model used was
the shallow water equations. The two space dimensions were
approximated using the linear FEM over triangular elements.
The time integration was performed using centered (Leap-frog)
finite differencing with consistent mass. Several grid
arrangements were attempted using well-behaved initial con-
ditions (wave number 1). The results displayed after 48 hours
of time integration were disappointing. There was mild im-
provement only with the addition of a diffusion term or when
a fine mesh was employed. They tested two different arrange-

ments of the diagonal slant of the triangular elements but did not identify whether the noise problems were associated with space or time differencing.

The FEM research at the Meteorological Office, Bracknell, England has been published by Cullen. His first work (Cullen, 1973) showed that the rectangular finite element with bilinear interpolation and consistent mass leap-frog time differencing results in a more restrictive (by a factor of $\sqrt{3}$) maximum time step than the one required when centered finite differencing is used. Additionally; he found that a 16 x 16 finite element grid gave results comparable to a 32 x 32 finite difference grid with second order differencing. His next publication (Cullen, 1974a) described his investigation of the shallow water equations using the same model problem as used by Grammeltvedt (1969). Cullen found that linear FEM approximation and triangular elements gave superior results to the finite difference models tested by Grammeltvedt. Specifically, the FEM handled wave number 1 to 5 (16 grid points along the channel) with 90 percent accuracy or better while the finite difference models with double the resolution only achieved 90 percent accuracy for wave numbers 1 to 3. Additionally, he found that his FEM model generated extraneous waves of two grid interval length.

Cullen (1974b) extended his work with the shallow water equations. The equations were expressed in spherical coordinates and were solved over a linear triangular mesh

where the globe was divided into large icosahedrons which were further subdivided into many small triangles. The resulting global grid had 1002 nodes (8-10 degrees apart). Initial conditions were the same as used by Phillips (1959) but because the icosahedral grid is unsymmetric, Cullen was forced to solve the system over the entire globe rather than over one octant as Phillips (1959) did. To discretize the time domain, Cullen used the Leap-frog method. Rather than using a pure FEM, Cullen added a 17-point spatial filter developed by Shapiro (1971). With this model, Cullen showed that the 1002-node finite element model performed better than a finite difference model using 4032 points. However, he did encounter noise problems in the model, especially at the intersections of the icosahedrons. He attributed the noise to the spatial discretization.

Because of the noise problems, Cullen (1976) continued his research by looking at the shallow water model in combination with artificial smoothing methods. Four smoothing schemes were tried, including fourth order nonlinear diffusion terms in all three equations, the Shapiro filter used in the previous paper (Cullen, 1976b), the addition of nonlinear diffusion terms in the u and v equations only and the Sadourney (1973) method. The latter method provided the best results. It is designed to damp the gravity waves.

In summary, it is clear that Cullen made important advances in the use of the FEM but it should be noted that

virtually all of his work was done using the linear triangular element with Leap-frog time differencing.

Some of the more advanced uses of the FEM are being made by the Atmospheric Environment Service of Canada. The principal researchers have been Staniforth, Mitchell, and Daley. Apparently, their original intent was to develop an operational regional baroclinic model using the FEM. Staniforth and Mitchell (1977) studied the use of semi-implicit time integration using the scheme of Kwizak and Robert (1971). That scheme was used in conjunction with a barotropic model where both bilinear and biquadratic interpolation functions were employed. Compared to the finite difference results of Kwizak and Robert, the FEM provided superior results especially in terms of noise reduction and reduced damping. The better FEM result was given by the quadratic interpolation functions; however, their further use was ruled out by the researchers because of the increased computational costs.

Staniforth and Daley (1977) expanded to a three-dimensional, primitive equation model where only the vertical coordinate was discretized using the FEM. The horizontal domain was approximated through an existing spectral model. Staniforth and Mitchell (1978) returned to the shallow water equations to investigate the effect of variable-resolution grids. They demonstrated that the forecast error is significantly reduced when a smoothly-varying mesh size is used to refine the grid rather than when the grid size changes

through a discrete jump. Within an area of interest the mesh size was held at a constant fine resolution and became more and more coarse away from that area. Again, for this problem they used the semi-implicit time integration scheme and bi-linear interpolation over rectangles. An interesting side-light to this research is their use of Simpson's rule for the element integrations rather than the more widely used Gauss quadrature method. Simpson's rule slightly compromises accuracy for faster speed.

The most recent paper by the Canadian group (Staniforth and Daley, 1979) describes a limited area, three-dimensional, baroclinic finite element model. The bilinear interpolation previously used was generalized to handle the three dimensional model. The model resolution was relatively coarse with seven levels in the vertical and 285 km between nodes in the fine mesh area. The results were encouraging, showing this model to be competitive with an operational 29 wave spectral model for forecast periods up to 48 hours.

In summary, this Canadian group has made advanced application of the FEM using the Kwizak and Robert semi-implicit time integration scheme with the bilinear finite element interpolation functions.

In contrast to the Canadian work on large scale models, the goal of researchers at the Lawrence Livermore Laboratory is to construct a three dimensional boundary layer model based on the FEM. Gresho, Lee, and Sani (1977) studied

the tradeoffs between lumped and consistent mass for linear

advection and diffusion problems. They found that when lump-

ed mass is employed, the phase speed and amplitude exhibit

much greater errors. They concluded that lumped mass "ser-

iously compromises the accuracy of the FEM" and recommended

that the effect of lumped mass be investigated for the non-

linear equations.

Huyakorn, et al. (1978) compared four elements (six-

node quadratic triangle as well as the four-, eight-, and

nine-node rectangles) using the mixed-order interpolation

method to investigate steady flow through a sudden expansion

and steady free thermal convection in a square cavity. Their

results showed that for those types of flow, the nine-node

Lagrangian element gave the best accuracy. They found that

the accuracy when using the six-node quadratic triangle was

highly dependent on the arrangement of the triangles. The

least accuracy was given by the eight-node serendipity ele-

ment. (see Appendix A for a discussion of the elements).

This result was used by Gresho, et al. (1978) to test a pre-

dictor-corrector method for time integration. The method

consisted of the Adams-Bashforth scheme as the predictor and

the trapezoidal rule as the corrector. The unique feature of

their algorithm is the provision for calculation of the time

truncation error and the subsequent adjustment of the time

step to reduce the error. This experiment was conducted using

mixed-order interpolation for flow starting from rest in a

channel with a sudden expansion. Lumped mass was again tried with much better results; however, this improvement was thought to be due to the much lower Reynold's number of the latter experiment.

Gresho, et al. (1978) summarize much of their earlier work on the Navier-Stokes equations for flow in a channel with a cylindrical obstruction. The major thrust of this work was to demonstrate the usefulness of their semi-implicit time differencing scheme described earlier.

Other related research accomplished by oceanographers includes a work by Fix (1975) dealing with mesoscale ocean flows. He described a simple vorticity-stream function model using quadratic and cubic triangular elements in space. No computational results are presented. Similar work is presented by Platzman (1978) who used a linearized set of primitive equations for a coarse resolution ocean circulation problem. His grid was identical to that of Cullen (1974b). Several papers dealing with tidal flow using the shallow water equations have been presented by Kawahara (1977 a, b, c). Interested in civil engineering aspects, he has modelled actual harbors, tributaries, and lakes using the FEM. The ease with which the FEM handles irregular boundaries such as Tokyo Harbor is amply demonstrated.

The research described above helps to define some of the large problem areas requiring investigation. Other than the research at Lawrence Livermore Laboratory, most of the

published works have described the use of a particular finite element (generally the linear triangle) with one time integration scheme.

At the University of Oklahoma, School of Meteorology, research was begun by looking closely at the FEM itself before applying the method to a sophisticated model. Using a finite difference equivalent to one of the FEM models tested here as well as some FDM models, Sasaki and Reddy (1977) studied several well-known time differencing schemes as well as the variational adjustment technique of Sasaki (1976). They did not specifically consider the concept of lumped and consistent mass but performed their testing using the FDM as it is normally formulated. They found that the FDM form of the bilinear FEM combined with the Crank-Nicholson time differencing scheme provided the best results. This scheme is, in fact, a consistent mass scheme; the others tested were not. Sasaki and Chang (1979) carried this work further by using a consistent mass operator with some of the finite difference schemes previously tested. They found improvement in the solution for each of the schemes when consistent mass was employed.

This research is a continuation of the work described above but is broader in scope. Here, the emphasis is on the FEM as it applies to the equations governing large scale flow in the atmosphere. Using advection-dominated flow with the nonlinear equations, the discussion which follows will provide

15

insight into the relative accuracies of several commonly used finite elements, the tradeoffs associated with several well-known time differencing schemes, the relative merits of lumped and consistent mass, and computational efficiency.

CHAPTER III

METHODOLOGY

Governing Equations and Finite Element Models

The objective of this study is to examine the FEM
approximation in space coupled with various time discretiza-
tion methods in order to determine the most accurate and
efficient application of the FEM for use in modelling the
large-scale flow of the atmosphere. Accordingly, three dif-
ferent models which describe flow in a channel will be used.
The first two models are derived from the following equation
set which describes inviscid, incompressible flow in a chan-
nel with no Coriolis force:

$$\frac{\partial u}{\partial t} + u\frac{\partial u}{\partial x} + v\frac{\partial u}{\partial y} + \frac{1}{\rho_0}\frac{\partial p}{\partial x} = 0,$$

$$\frac{\partial v}{\partial t} + u\frac{\partial v}{\partial x} + v\frac{\partial v}{\partial y} + \frac{1}{\rho_0}\frac{\partial p}{\partial y} = 0,$$
(1)

$$\frac{\partial u}{\partial x} + \frac{\partial v}{\partial y} = 0.$$
(2)

Here u and v are the velocity components in the x and y dir-
ections respectively, ρ_0 is the constant density, p is the
pressure, t is the time, and (x,y) denotes a point in Ω, an
open bounded region in two-dimensional Euclidean space with

17

boundary denoted by $\partial\Omega$.

Vorticity - Stream Function FEM Model

The first model investigated is the vorticity-stream function model. The stream function (ψ) is defined by

$$u = -\frac{\partial\psi}{\partial y}, \quad v = \frac{\partial\psi}{\partial x} . \tag{3}$$

The vorticity (ζ) is given by

$$\zeta = \frac{\partial v}{\partial x} - \frac{\partial u}{\partial y} . \tag{4}$$

The use of the stream function automatically satisfies (2) so that (1), (2), (3), and (4) may be combined giving

$$\frac{\partial\zeta}{\partial t} + J(\psi,\zeta) = 0 ,$$

$$\nabla^2\psi = \zeta , \tag{5}$$

where $J(\psi,\zeta) \equiv \frac{\partial\psi}{\partial x} \frac{\partial\zeta}{\partial y} - \frac{\partial\psi}{\partial y} \frac{\partial\zeta}{\partial x}$ is the Jacobian operator.

If the domain Ω is subdivided into small elements, Ω_e the vorticity and stream function may be approximated over an element (e) by

$$\zeta^e = \sum_i \zeta_i^e N_i \text{ and } \psi^e = \sum_i \psi_i^e N_i . \tag{6}$$

Here, the subscript i denotes the node or grid point i and N_i represents the element interpolation or shape functions. The interpolation functions have the property that all but one are zero at a given node; the one corresponding to that.

18

node is unity. Using (6), the application of the Galerkin method to (5) results in

$$\iint_{\Omega_e} \{ \frac{\partial \zeta^e}{\partial t} + J(\psi^e, \zeta^e) \} \, N_i \, dx \, dy = 0,$$

$$\iint_{\Omega_e} \{ \frac{\partial \psi^e}{\partial x} \frac{\partial N_i}{\partial x} + \frac{\partial \psi^e}{\partial y} \frac{\partial N_i}{\partial y} + \zeta N_i \} \, dx \, dy = 0 . \tag{7}$$

Therefore, over an element Ω_e,

$$[M^e] \{ \frac{\partial \zeta^e}{\partial t} \} + [J^e] \{ \zeta^e \} = 0, \tag{8}$$

$$[K^e] \{ \psi^e \} + [M^e] \{ \zeta^e \} = 0, \tag{9}$$

where $\displaystyle M_{ij}^e = \iint_{\Omega_e} N_i N_j \, dx \, dy$,

$$J_{ij}^e = \iint_{\Omega_e} N_i \{ \frac{\partial \psi^e}{\partial x} \frac{\partial N_j}{\partial y} - \frac{\partial \psi^e}{\partial y} \frac{\partial N_j}{\partial x} \} \, dx \, dy,$$

$$K_{ij}^e = \iint_{\Omega_e} \{ \frac{\partial N_i}{\partial x} \frac{\partial N_j}{\partial x} + \frac{\partial N_i}{\partial y} \frac{\partial N_j}{\partial y} \} \, dx \, dy .$$

It should be noted that the matrices $[M^e]$ called consistent mass matrix and $[K^e]$ are constant and need to be computed and stored only once for each element; however, the nonlinear matrix $[J^e]$ must be recomputed on each iteration and/or time step, depending on the time integration scheme used. Computational details are given in later sections of this chapter.

Penalty FEM

An alternative to the vorticity - stream function formulation of (1) and (2) is the penalty method, which is

19

also known as the weak-constraint method (Courant, 1943 and Reddy, 1979a, b). In the penalty method, (1) are taken to be the governing equations and (2) is the constraint. Expressing (1) in the variational form gives

$$\delta I(u, v; \delta u, \delta v) = \iint \{ [\frac{\partial u}{\partial t} + u\frac{\partial u}{\partial x} + v\frac{\partial u}{\partial y}]\ \delta u + \frac{1}{\rho_o}\frac{\partial P}{\partial x}\ \delta u$$

$$+ [\frac{\partial v}{\partial t} + u\frac{\partial v}{\partial x} + v\frac{\partial v}{\partial y}]\ \delta v + \frac{1}{\rho_o}\frac{\partial P}{\partial y}\ \delta v \}\ \ dx\ dy, \tag{10}$$

where δI represents the first variation of the functional I with respect to u and v and δu and δv are the variations of u and v respectively. Application of Green's theorem, a generalization of the integration by parts gives

$$\delta I(u, v; \delta u, \delta v) = \iint \{ [\frac{\partial u}{\partial t} + u\frac{\partial u}{\partial x} + v\frac{\partial u}{\partial y}]\delta u + [\frac{\partial v}{\partial t} + u\frac{\partial v}{\partial x} + v\frac{\partial v}{\partial y}]\ \delta v$$

$$- \frac{P}{\rho_o}\ \delta(\frac{\partial u}{\partial x} + \frac{\partial v}{\partial y}) \}\ dx\ dy + \oint_{\partial\Omega} [t_x\delta u + t_y\delta v]\ dS. \tag{11}$$

Here $t_x = \frac{P}{\rho_o} n_x$, $t_y = \frac{P}{\rho_o} n_y$, and (n_x, n_y) are the components of the unit normal to the boundary $\partial\Omega$. The integration by parts resulted in the boundary term which requires that either the tractions (t_x and t_y) or the variations of u and v be specified on $\partial\Omega$. For this problem, u and v are held constant on $\partial\Omega$ making $\delta u = 0$ and $\delta v = 0$ on the boundary $\partial\Omega$. With this specification and after substituting (2), the expression (11) reduces to

$$\delta I(u, v; \delta u, \delta v) = \iint \{ [\frac{\partial u}{\partial t} + u\frac{\partial u}{\partial x} + v\frac{\partial u}{\partial y}]\ \delta u$$

$$+ [\frac{\partial v}{\partial t} + u\frac{\partial v}{\partial x} + v\frac{\partial v}{\partial y}]\delta v \}\ dx\ dy. \tag{12}$$

The substitution of the constraint (2) above does not insure that non-divergence will be satisfied; therefore, it is added to the variational form (12) as a weak constraint. This is analogous to the weak constraint method described by Sasaki (1970a,b). Adding the weak constraint to (12) gives

$$\delta I(u,v;\delta u,\delta v) = \iint_{\Omega} \{ [\frac{\partial u}{\partial t} + u\frac{\partial u}{\partial x} + v\frac{\partial u}{\partial y}] \, \delta u + [\frac{\partial v}{\partial t} + u\frac{\partial v}{\partial x} + v\frac{\partial v}{\partial y}] \, \delta v$$

$$+ \lambda(\frac{\partial u}{\partial x} + \frac{\partial v}{\partial y})(\frac{\partial}{\partial x}\delta u + \frac{\partial}{\partial y}\delta v) \} \, dx \, dy, \tag{13}$$

where λ is the penalty parameter (or weight).

In order that the functional I attains its minimum it is necessary that $\delta I = 0$. It should be noted that in (13), the pressure has been eliminated as a variable so that the number of unknowns has been reduced to two. By finding the Euler-Lagrange equations for (10) and (13) and then equating the like terms, one can find the following relationship for the pressure (Reddy, 1979b).

$$\lim_{\lambda \to \infty} \lambda \, (\frac{\partial u_\lambda}{\partial x} + \frac{\partial v_\lambda}{\partial y}) = -P. \tag{14}$$

This is based on the fact that as the penalty parameter (λ) approaches infinity, the solution (u_λ, v_λ) to (13) provides an approximation to the pressure based on the chosen value for λ. This is the 'penalty' resulting from the elimination of pressure as a variable.

For the penalty finite element method, the velocity components are approximated as in (6):

21

$$u^e = \sum_i u^e_i N_i \quad \text{and} \quad v^e = \sum_i v^e_i N_i. \tag{15}$$

substitution of (15) into (13) gives the semidiscrete Galerkin form

$$\iint\limits_{\Omega_e} \left\{ \left[\frac{\partial u^e}{\partial t} + u^e \frac{\partial u^e}{\partial x} + v^e \frac{\partial u^e}{\partial y} \right] N_i + \left[\frac{\partial v^e}{\partial t} + u^e \frac{\partial v^e}{\partial x} + v^e \frac{\partial v^e}{\partial y} \right] N_i \right.$$
$$\left. + \lambda \left(\frac{\partial u^e}{\partial x} + \frac{\partial v^e}{\partial y} \right) \left(\frac{\partial N_i}{\partial x} + \frac{\partial N_i}{\partial y} \right) \right\} dx\, dy = 0. \tag{16}$$

The computational form for (16) is

$$[C^e]\, \{\dot{\Delta}^e\} + [[K^e] + \lambda [P^e]]\, \{\Delta^e\} = \{0\}, \tag{17}$$

where

$$[C^e] = \begin{bmatrix} [M^e] & [0] \\ [0] & [M^e] \end{bmatrix}, \quad [K^e] = \begin{bmatrix} [A^e] & [0] \\ [0] & [A^e] \end{bmatrix},$$

$$[P^e] = \begin{bmatrix} [S^{xx}] & [S^{xy}] \\ [S^{xy}] & [S^{yy}] \end{bmatrix}, \quad M_{ij} = \iint\limits_{\Omega_e} N_i N_j\, dx\, dy,$$

$$A_{ij} = \iint\limits_{\Omega_e} \left[u_e N_i \frac{\partial N_j}{\partial x} + v_e N_i \frac{\partial N_j}{\partial y} \right] dx\, dy,$$

$$S^{xx}_{ij} = \iint\limits_{\Omega_e} \frac{\partial N_i}{\partial x} \frac{\partial N_j}{\partial x} dx\, dy, \quad S^{yy}_{ij} = \iint\limits_{\Omega_e} \frac{\partial N_i}{\partial y} \frac{\partial N_j}{\partial y} dx\, dy,$$

$$S^{xy}_{ij} = \iint\limits_{\Omega_e} \frac{\partial N_i}{\partial x} \frac{\partial N_j}{\partial y} dx\, dy.$$

For computation, matrices $[C^e]$ and $[P^e]$ need be computed and

stored for each element only one time, matrix $[K^e]$ is non-linear and must be recomputed on every time step and/or iteration.

Finite Element Model of Shallow Water Equations

The models described above provide a good test of the ability of the FEM to handle the nonlinear effects, which are important terms in the governing equations of the atmosphere; however, one great difficulty in operational numerical weather prediction is the occurence of fast-moving waves such as gravity waves. Models must be able to handle these waves without their energy increasing and consequently destroying the forecast. A good model to test these effects is the well known shallow water model. The shallow water equations in u and v are the same as (1) except that the Coriolis term appears. The third equation which governs the height of the free fluid surface results from integration of the continuity equation in the vertical (Haltiner, 1971). The shallow water equations are given by

$$\frac{\partial u}{\partial t} + u\frac{\partial u}{\partial x} + v\frac{\partial u}{\partial y} + g\frac{\partial h}{\partial x} - fv = 0,$$

$$\frac{\partial v}{\partial t} + u\frac{\partial v}{\partial x} + v\frac{\partial v}{\partial y} + g\frac{\partial h}{\partial y} + fu = 0,$$

$$\frac{\partial h}{\partial t} + u\frac{\partial h}{\partial x} + v\frac{\partial h}{\partial y} + h(\frac{\partial u}{\partial x} + \frac{\partial v}{\partial y}) = 0.$$

(18)

Here f is the Coriolis term, h is the height of the free surface of the fluid, and g is gravitational acceleration.

23

The semidiscrete Galerkin form of (18) is

$$\iint_{\Omega_e}\{[\frac{\partial u^e}{\partial t} + u^e\frac{\partial u^e}{\partial x} +v^e\frac{\partial u^e}{\partial y}] N_i +g\frac{\partial h^e}{\partial x} N_i -fv^e N_i\} \, dx \, dy = 0,$$

$$\iint_{\Omega_e}\{[\frac{\partial v^e}{\partial t} + u^e\frac{\partial v^e}{\partial x} + v^e\frac{\partial v^e}{\partial y}] N_i +g\frac{\partial h^e}{\partial y} N_i + fu^e N_i\} dx \, dy=0,$$

$$\qquad\qquad\qquad\qquad\qquad\qquad\qquad\qquad\qquad (19)$$

$$\iint_{\Omega_e}\{[\frac{\partial h^e}{\partial t} +u^e\frac{\partial h^e}{\partial x} +v^e\frac{\partial h^e}{\partial y}] N_i + h^e[\frac{\partial u^e}{\partial x} + \frac{\partial v^e}{\partial y}] N_i\} dx \, dy=0.$$

If u, v, and h are approximated over a typical element by u^e = $\sum_i u_i^e N_i$, $v^e= \sum_i v_i^e N_i$, and $h^e= \sum_i h_i^e N_i$ then (19) becomes

$$[M^e] \{\dot{u}^e\} + [A^e] \{u^e\} = \{F_u\} \ ,$$

$$[M^e] \{\dot{v}^e\} + [A^e] \{v^e\} = \{F_v\} \ , \qquad\qquad (20)$$

$$[M^e] \{\dot{h}^e\} + [L^e] \{h^e\} = \{0\} \ ,$$

where

$$M_{ij}^e= \iint_{\Omega_e}N_i N_j \, dx \, dy, \quad A_{ij}^e = \iint_{\Omega_e}N_i\{u^e \frac{\partial N_j}{\partial x} + v^e\frac{\partial N_j}{\partial x}\} \, dx \, dy,$$

$$F_{u_i} = \sum_j\{f M_{ij}^e v_j^e - g[\iint_{\Omega_e}N_i \frac{\partial N_j}{\partial x} \, dx \, dy] hj\} \ ,$$

$$F_{v_i} = \sum_j\{-f M_{ij}^e u_j^e - g[\iint_{\Omega_e} N_i \frac{\partial N_j}{\partial y} \, dx \, dy] h_j^e\},$$

$$L_{ij}^e = A_{ij}^e + \iint_{\Omega_e} N_i N_j (\frac{\partial u^e}{\partial x} + \frac{\partial v^e}{\partial y}) \, dx \, dy.$$

The only matrix in (20) which does not change is $[M^e]$. All others must be recomputed for each element on each iteration

and/or time step.

The matrix equations (8), (17), and (20) are a result of the general application of the FEM. At this point a general computer program could be written for each model. Once the general program is developed, consideration must be given to actual space and time discretization which includes the development of the element interpolation functions. The final steps are the selection of the actual mesh for the domain of the model and the imposition of the specific initial and boundary conditions required for the solution. The discussion which follows details the approach taken in each of these areas for the three models considered.

Numerical Procedure

Space Discretization

The finite element method involves the approximation of functions over subdomains (Ω_e) of the global domain (Ω). The possible shapes of these subdomains or elements are limitless; however, unusual or completely irregular shapes are difficult to manage and their corresponding interpolation functions are not easily obtainable. The most widely used element shapes in two dimensional finite element analysis are the triangle and rectangle. The order of the interpolation functions used determines the number and placement of nodal points within the element shape.

In this study five different elements are tested: the three-node linear triangle, the four-node bilinear rectangle, the six-node quadratic triangle, the eight-node quadratic rectangle, and the nine-node quadratic rectangle. The eight- and nine-node elements both use quadratic interpolation but the interpolation functions are developed in different ways. The determination of the interpolating functions is discussed in Appendix A. These interpolating functions correspond to the term N_i shown in (6, 7, 8, 9, 15, 16, 19, and 20) so that the semi-discrete form of the equations is developed independent of the element choice and is then general for any element application.

For the problem discussed here, the element size is

held constant throughout the domain of the problem. This has many simplifying effects on the calculations and greatly reduces computer storage requirements since element matrices such as $[M^e]$ in (20) need be calculated for only one element and stored rather than for each element. In a model with complex boundaries or where grid refinement is desired this savings is not possible.

When the element size is constant it is possible to reduce the FEM to a finite difference form; however, the resulting finite difference form will be valid only for an interior grid point and special considerations must be made near the boundaries. Jesperson (1974) developed a finite difference form for the vorticity - stream function equation (8) using the bilinear rectangle finite element approximations. The resulting finite difference equation is given by

$$\frac{1}{36} [16\dot{\zeta}_{ij} + 4(\dot{\zeta}_{i+1,j} + \dot{\zeta}_{i-1,j} + \dot{\zeta}_{i,j+1} + \dot{\zeta}_{i,j-1}) +$$

$$\dot{\zeta}_{i+1,j+1} + \dot{\zeta}_{i+1,j-1} + \dot{\zeta}_{i-1,j+1} + \dot{\zeta}_{i-1,j-1}]$$

$$= \frac{1}{12d^2} [(\psi_{i,j+1} - \psi_{i+1,j})\zeta_{i+1,j+1} + (\psi_{i-1,j} - \psi_{i,j+1})\zeta_{i-1,j+1}$$

$$+ (\psi_{i+1,j} - \psi_{i,j-1})\zeta_{i+1,j-1} + (\psi_{i,j-1} - \psi_{i-1,j})\zeta_{i-1,j-1}$$

$$+ (\psi_{i,j+1} - \psi_{i,j-1} + \psi_{i+1,j+1} - \psi_{i+1,j-1})\zeta_{i+1,j}$$

$$+ (\psi_{i,j-1} - \psi_{i,j+1} + \psi_{i-1,j-1} - \psi_{i-1,j+1})\zeta_{i-1,j}$$

$$+ (\psi_{i+1,j} - \psi_{i-1,j} + \psi_{i+1,j-1} - \psi_{i-1,j-1})\zeta_{i,j-1}$$

$$+ (\psi_{i-1,j} - \psi_{i+1,j} + \psi_{i-1,j+1} - \psi_{i+1,j+1})\zeta_{i,j+1}]$$

$$(21)$$

where d is the spacing between grid points and the subscripts indicate the grid point. As noted by Jesperson, the right side of (21) is identical to the well-known Arakawa Jacobian; however, this expression for the Jacobian was developed in a completely different way by Arakawa (1966).

In this study, the results using (21) as well as a simple centered space finite difference scheme are compared to the results using the five different finite elements. The left side of (21) will be discussed in a later section dealing with consistent and lumped mass.

Time Discretization

Several time differencing schemes have been used for comparison of their effects on the solution. The Crank-Nicholson scheme was chosen as the basis of comparison for the different finite element discretizations because it has neutral stability, no computational mode, and therefore should have no effect on the phase speed or the amplitude of the solution (Mesinger and Arakawa, 1976). The major drawback to this scheme is that it is fully implicit and requires iteration at each time step. The Crank-Nicholson method is included in a family of schemes known as the θ-family of approximations (Zienkiewcz, 1977) which may be expressed by

$$\{q\}^{n+1} = \{q\}^n + \theta \Delta t \, \{\dot{q}\}^{n+1} + (1-\theta) \, \Delta t \{\dot{q}\}^n \, , \qquad (22)$$

where the superscript indicates the time $(t=n\Delta t)$, $\{q\}$ is the unknown function, Δt is the time step, and θ determines the specific scheme. For example, some of the possible schemes are,

$\theta = 0$, Forward (Euler),

$\theta = 1/2$, Crank-Nicholson,

$\theta = 2/3$, Galerkin, and

$\theta = 1$, Backward.

Of these four schemes, all were used except the Forward differencing scheme which was eliminated because linear stability analysis indicates that it is always unstable. All of the remaining schemes are fully implicit. The Galerkin and Backward methods both damp the amplitude of the solution with the greater damping occurring in the Backward scheme. In addition, two explicit schemes will be used: the well-known Leap-frog or centered scheme which is given by

$$\{q\}^{n+1} = \{q\}^{n-1} + 2\Delta t \; \{\dot{q}\}^n \; , \tag{23}$$

and the Matsuno scheme which is a two-step method given by

$$\{q\}^{n+1*} = \{q\}^n + \Delta t \; \{\dot{q}\}^n$$

$$\{q\}^{n+1} = \{q\}^n + \Delta t \; \{\dot{q}\}^{n+1*} , \tag{24}$$

The Matsuno scheme results in damping of the solution. The Leap-frog scheme suffers from the presence of the computational mode which restricts the choice of time step.

This restriction may be determined by applying the von Neumann stability analysis to a linearized form of the advective equation (Mesinger and Arakawa, 1976). For a centered finite difference scheme applied to the linear version of (5) the von Neumann technique gives the well known CFL criteria for stability:

$$\sqrt{2} \ \frac{c\Delta t}{d} \leq 1, \tag{25}$$

where c is the phase speed of the wave and the factor $\sqrt{2}$ is present for the two-dimensional problem. When the FEM is applied to the linear version of (5) and the four-node bilinear element is used with Leap-frog time differencing the time step restriction is

$$\sqrt{2} \ \frac{c\Delta t}{d} \leq \frac{1}{\sqrt{3}} \tag{26}$$

Thus, the FEM imposes a penalty of $\sqrt{3}$ on the time step (Cullen, 1974). The time step penalty results because of the coupling of the time derivative through the mass matrix. Some detailed stability analyses are given in Appendix B.

This coupling of the time derivative shown by the left side of (21) is known as consistent mass. Physically, (21) states that the advection which is calculated by the right side of the equation for the node (i,j) affects the time derivative not only at that node but also at the surrounding nodes. In contrast, when lumped mass is used the left side of (21) degenerates to a single term $(\dot{\zeta}_{i,j})$. The resulting equation

30

is the traditional approach taken in finite difference methods and as shown here and by Sasaki and Chang (1979), the results using (21) are much more accurate than the traditional finite difference approach. As discussed by Zienkiewicz (1977) there are several approaches to lumping the mass in the FEM; however, the simplest method is to make the matrix $[M^e]$ in (8), (17), and (20) diagonal. The latter method is used in this study. The choice of lumped or consistent mass greatly affects the computational details of the problem being considered. Computational details will be discussed in the following section.

Computational Details

The vorticity equation (8) combined with Crank-Nicholson time differencing may be written as either

$$\left[[M] + \frac{\Delta t}{2} [J]^{n+1}\right] \{\zeta\}^{n+1} = \left[[M] - \frac{\Delta t}{2} [J]^n\right] \{\zeta\}^n, \quad (27)$$

$$\text{or } [M] \{\Delta\zeta\} = \{F\}, \quad (28)$$

where $\{F\} = -\frac{\Delta t}{2} [J]^{n+1} \{\zeta\}^{n+1} + \left[[M] - \frac{\Delta t}{2} [J]^n\right] \{\zeta\}^n$,

$$\{\zeta\}^{n+1} = \{\zeta\}^n + \{\Delta\zeta\}.$$

From an algebraic point of view (27) and (28) are equivalent equations; however, computationally they are quite different. When solving (27), the right side of the equation is known. The matrix $[J]^{n+1}$ is not known since it depends on the stream

31

function at the new time. The procedure for solving (27) is to calculate the right side, then calculate $[J]^{n+1}$ based on a guess, then solve for $\{\zeta\}^{n+1}$. The stream function equation (9) is then solved for $\{\psi\}^{n+1}$. These new values of ψ serve as the guess in the following iteration. The iterative process is repeated until the solution converges. The coefficient matrix on the left is recomputed for each element on each iteration and assembled into the global matrix which is banded and unsymmetric. The result is a set of linear algebraic equations which must be solved for $\{\zeta\}^{n+1}$. The latter task is extremely time consuming for the computer, especially when the number of nodes is large.

The alternative is to use (28). The matrix $[J]^{n+1}$ must still be computed but it is multiplied by a guess (values from the previous iteration) for $\{\zeta\}^{n+1}$ and placed into the force vector. The coefficient matrix $[M]$ is banded and symmetric. It must be calculated only once and can be decomposed once using Cholesky decomposition (Carnahan, et al., 1969). Then on each iteration, only forward and backward substitution are required to calculate the solutions. Even though the number of iterations required for convergence may be greater for (28) than for (27), the overall time savings can be substantial.

When using an explicit time differencing method the resulting form is similar to (28) and the set of algebraic equations can be solved as in (28) with no iteration. The

latter point makes the Leap-frog differencing scheme very attractive computationally. If lumped mass is used the matrix [M] becomes diagonal and the solution of (28) is relatively simple and fast. The combination of lumped mass and (27) results in little, if any, savings. Specific results from each method will be discussed in Chapter IV.

The Model Problem

For the vorticity-stream function model the domain chosen is a channel, 3800 km in length and width.

The initial conditions for the stream function are given by

$$\psi^*(x,y) = -U_o y - \psi_o \exp[-a(x^2+y^2)], \qquad (29)$$

where U_o, ψ_o, and a are constants and the origin is at the center of the domain. This model problem is identical to the one used by Sasaki and Reddy (1979) and Sasaki and Chang (1979) and is used here to facilitate comparison of results. The initial conditions for vorticity were derived by appropriate differentiation of (29). These initial conditions are shown in Fig. 1. The boundary conditions are

$$\left.\begin{array}{l}\psi(0,y) = \psi(L,y), \\ \zeta(0,y) = \zeta(L,y),\end{array}\right\} \quad \text{east-west boundaries}$$

$$\left.\begin{array}{l}\psi(x,0) = C_1, \\ \psi(x,W) = C_2,\end{array}\right\} \quad \text{north-south boundaries}$$
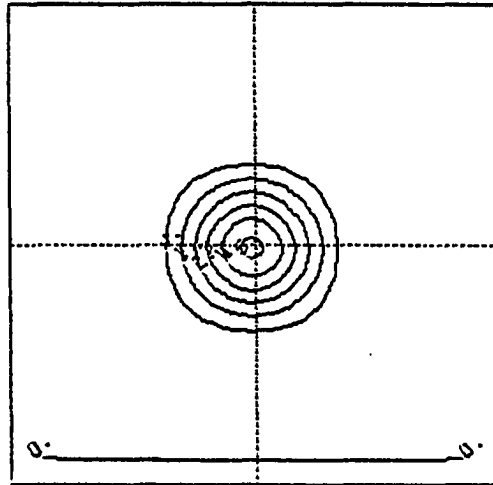
VORTICITY (S⁻¹)
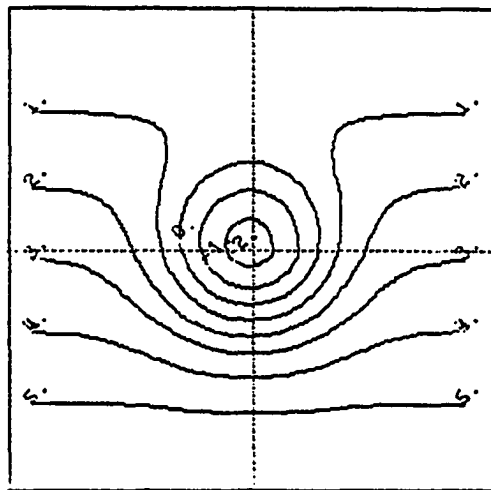
STREAM FUNCTION (M²/S)

Fig. 1. Initial conditions for ψ/ζ

where the channel length is L, W is the width, and C_1 and C_2 are constants. For these initial and boundary conditions, the model equations (5) have a unique analytical solution.

$$\psi(x,y,t) = \psi^*(x-U_o t,y). \tag{30}$$

The solution indicates that the circular vortex propagates eastward until it reappears on the west edge and returns to its initial position after a period of L/U_o. For the constants chosen here, that period is exactly 120 hours.

For the penalty method, the initial conditions are obtained by using the definition (3) and the initial conditions for stream function (29). The resulting initial conditions for u and v describe the same circular vortex. These initial conditions are shown in Fig. 2. As long as the proper value for the penalty parameter (λ) is chosen, the behavior of the vortex should be similar to the behavior experienced in the vorticity - stream function model. The boundary conditions used are

$$u(0,y) = u(L,y),$$
$$v(0,y) = v(L,y),$$

east-west boundaries

$$u(x,o) = u(x,W) = U_o,$$
$$v(x,o) = v(x,W) = 0.$$

north-south boundaries

Here the u and v components must both be specified because of the boundary term which appears in (11).

In the shallow water equation model, the domain and
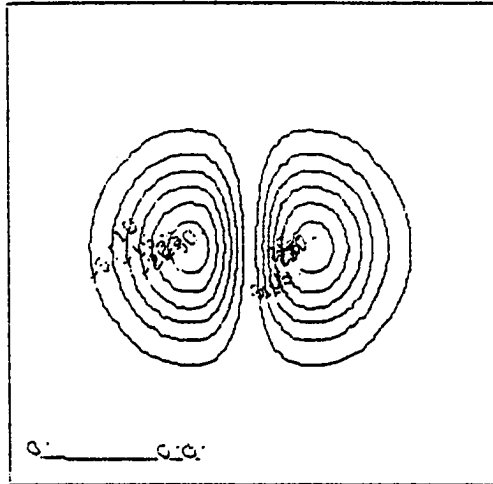
V COMPONENT OF WIND (M/S)
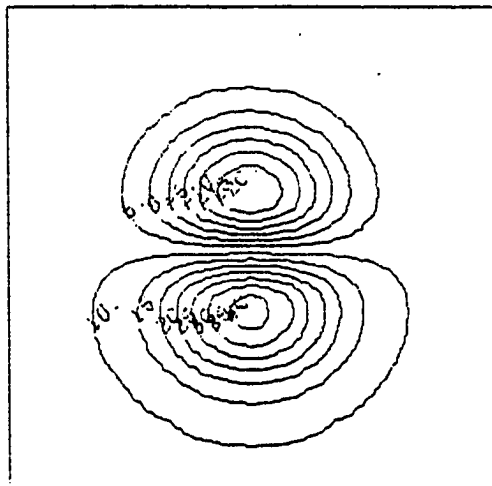
U COMPONENT OF WIND (M/S)

Fig. 2.   Initial conditions for penalty method

initial conditions chosen are the same as used by Grammelt-
vedt (1969) and later by Cullen (1974a). The domain is a
channel 6000 km in length and 4400 km wide. The initial
conditions are

$$h(x,y) = H_o + H_1 \cdot \tanh \frac{9(y-y_o)}{2W} + H_2 \cdot \text{sech}^2 \frac{9(y-y_o)}{W} \quad .$$

$$[0.8 \sin (\frac{2\pi x}{L}) + 0.5 \sin (\frac{6\pi x}{L})] , \tag{30}$$

where

$$H_o = 2000 \text{ m,} \qquad\qquad L = 6000 \text{ km,}$$

$$H_1 = -220 \text{ m,} \qquad\qquad W = 4400 \text{ km,}$$

$$H_2 = 133 \text{ m,} \qquad\qquad Y_o = W/2,$$

$$g = 10 \text{ ms}^{-2}.$$

The initial conditions for u and v are determined using the
FEM with the geostrophic relation,

$$u = -\frac{g}{f} \frac{\partial h}{\partial y} \text{ and } v = \frac{g}{f} \frac{\partial h}{\partial x} \quad .$$

The 'Beta-plane' approximation is made where-in the Coriolis
parameter (f) is calculated from

$$f = f_o + \beta y ,$$

where $f_o = 1.0 \cdot 10^{-4} s^{-1}$ and $\beta = 1.5 \cdot 10^{-11} s^{-1} m^{-1}$. These initial
conditions are shown in Fig. 3. Physically, these initial
conditions describe a west to east jet-stream which has north-
south disturbances along its axis (Grammeltvedt, 1969). The
initial conditions are shown in Fig. 3. The boundary condi-

37
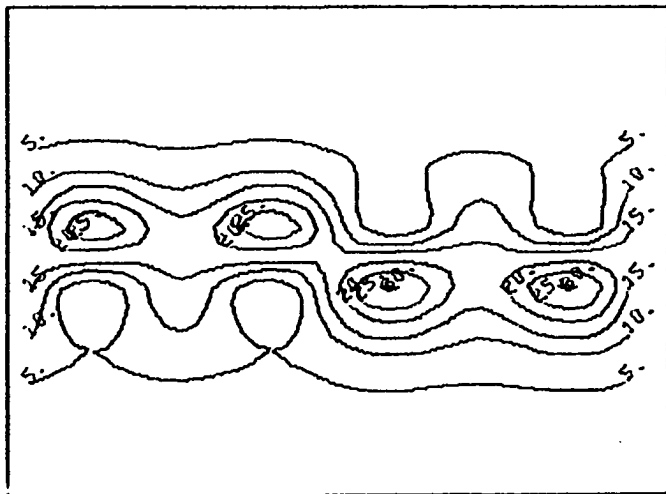
U COMPONENT OF WIND (M/S)
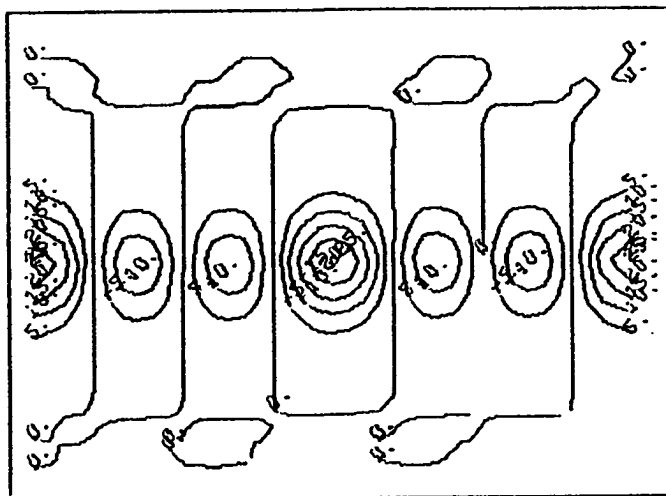
V COMPONENT OF WIND (M/S)
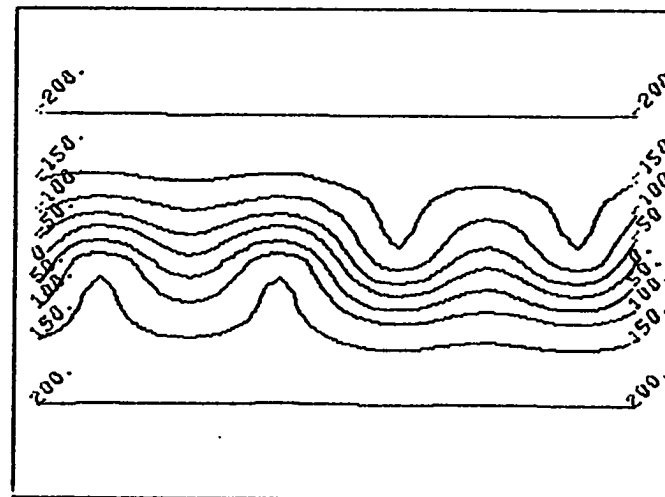
HEIGHT FIELD (M)

Fig. 3. Initial conditions for the shallow water equations

tions specified for this model are

$$u(0,y) = u(L,y),$$
$$v(0,y) = v(L,y),$$ east-west boundary
$$h(0,y) = h(L,y),$$
$$v(x,0) = v(x,W) = 0.$$ north-south boundary

It is interesting to note that there is a subtle difference between the north-south boundary conditions specified here and those required in finite difference models. Grammeltvedt (1969) was forced to specify boundary conditions for all variables in his models; this is an overspecification in a continuous model and sometimes called numerical boundary conditions. This additional specification at the boundaries can adversely effect the solution (Sundström, 1973).

The Grid (Finite Element Mesh)

Both the vorticity-stream function and penalty models are solved on an evenly-spaced grid consisting of 11 x 11 nodal points with 380 km spacing. For the shallow water equations, a grid of 15 x 21 nodal points is employed with 300 km spacing in the east-west direction and approximately 315 km spacing in the north-south direction. In order to impose periodic boundary conditions in the FEM, the nodal values on the eastern boundary are considered to be identical to those on the western boundary but their locations are preserved.

As stated earlier, linear and quadratic rectangular

as well as triangular elements are tested for their relative accuracy. Regardless of the element type (i.e., rectangular with four-or nine-nodes, or triangular with three-or six-nodes), the number of elements chosen is such that the total number of nodes remains the same. That is, one nine-node quadratic element replaces four bilinear four-node elements; or, two three-node linear triangular elements replace one four-node linear element, etc. However, when an eight-node quadratic (serendipity) element is used (the center node is missing when compared to the nine-node element), the total number of nodes is reduced. In the case of the vorticity-stream function model, the total number of nodes is reduced from 121 to 96. Fig. 4 shows the relative size and arrangement of the elements used. Both the three-and six-node triangles shown in Fig. 5 have been tested with the vorticity-stream function model. These results are presented in Chapter IV.

Accuracy Indicators

The results from the vorticity-stream function and penalty models using the different time and space discretizations discussed are compared for lumped versus consistent mass, position of the nonlinear terms, convergence rate, program size, computer time, and accuracy of the solution. Other than accuracy, all the comparisons are straight forward. The root-mean-sqaure error (RMSE), given by

40
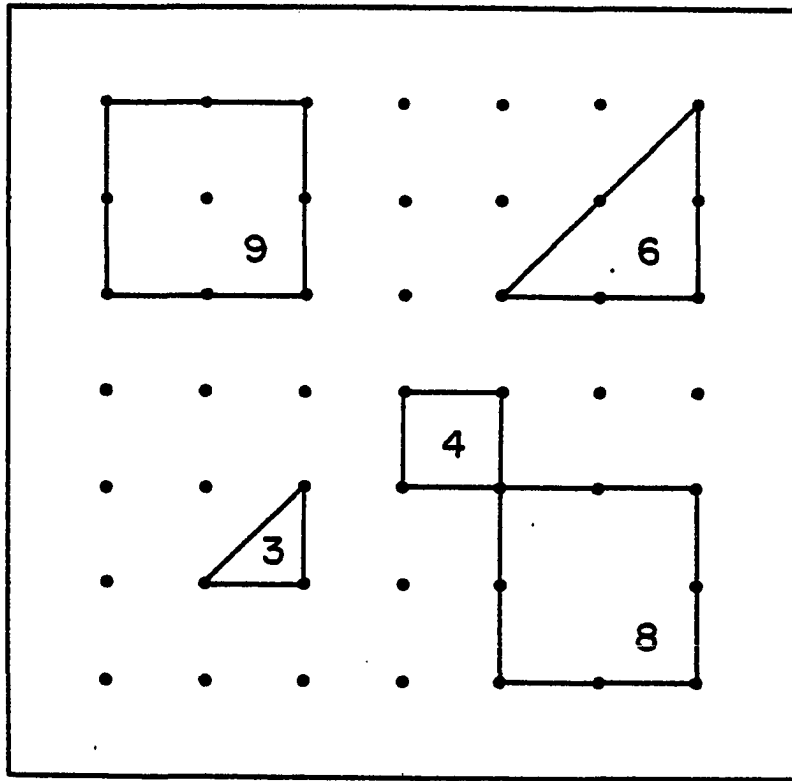
Fig. 4.   Arrangement of elements within
the mesh.
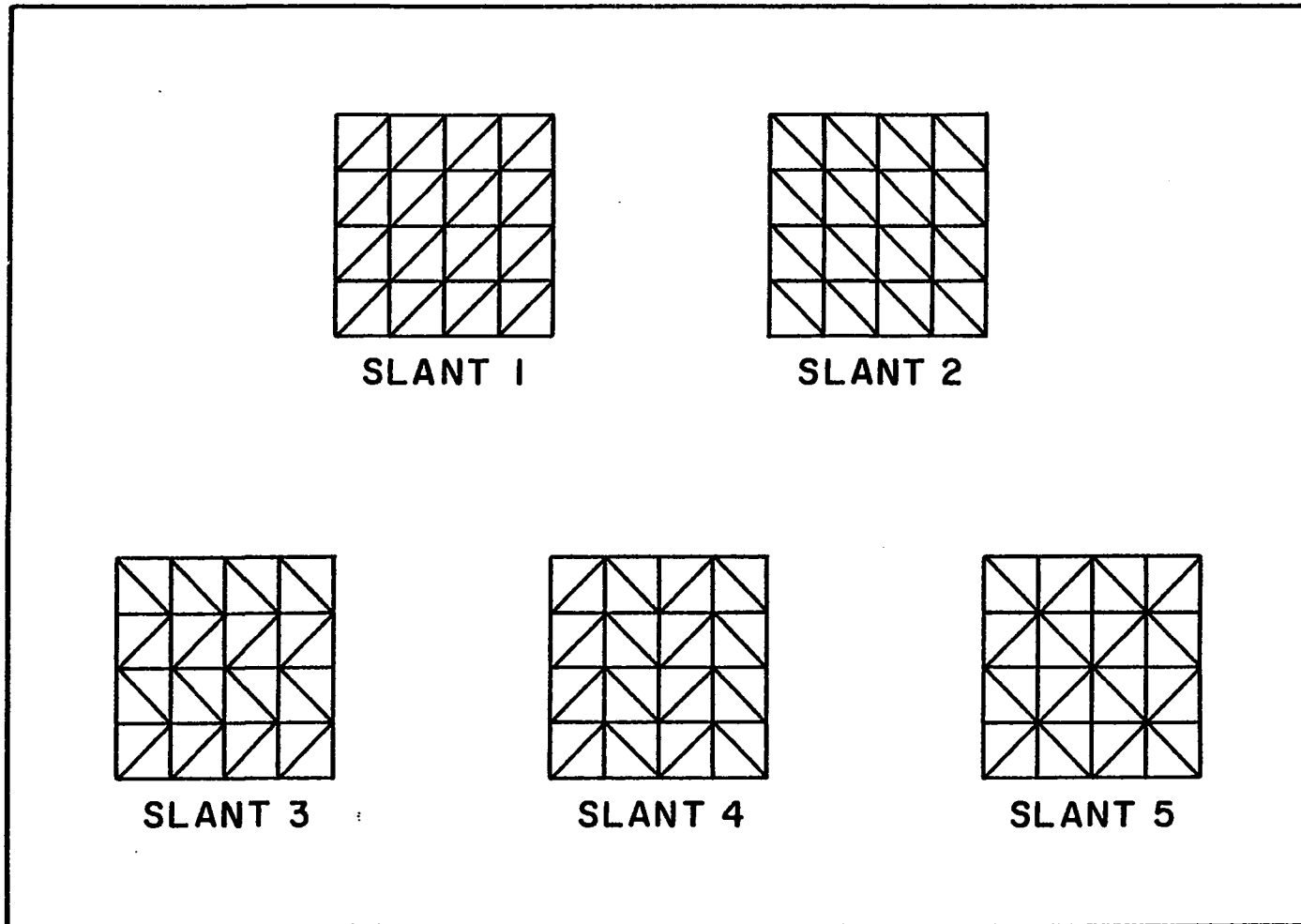
Fig. 5.   Arrangement of triangular elements within the mesh

$$RMSE = \frac{\Sigma (F_i - S_i)^{\frac{1}{2}}}{N}$$

where N is the number of grid points, F_i are the forecast values, and S_i are the solution values, is used as the basis of comparison for accuracy. This measure can be misleading if used alone. Here the RMSE is combined with visual examination of the analytical solution and 120 hour forecast fields of the vorticity and stream function.

Comparisons of the results from the shallow water equation model are more complicated since the equations are non-linear and there is no analytical solution. However, there are some facts about the model which can be checked and compared.

The absolute vorticity, and the total energy are conserved in the FEM model. Another parameter conserved in the FEM model is the mean wave number (Cullen, 1974b). Because of this, the allocation of energy among wave numbers should not change significantly during the forecast. Therefore, a two dimensional Fourier analysis has been performed on the initial height fields as well as the 48-hour forecast height fields. These analyses are based on a discussion by Goodman (1968) and calculated using an algorithm developed by Duchon[1]. Fig. 6 shows the two-dimensional Fourier analysis of the initial height field. This three dimensional plot shows the

---

[1]Associate Professor C.E. Duchon, School of Meteorology, University of Oklahoma provided a copy of the algorithm for this work.
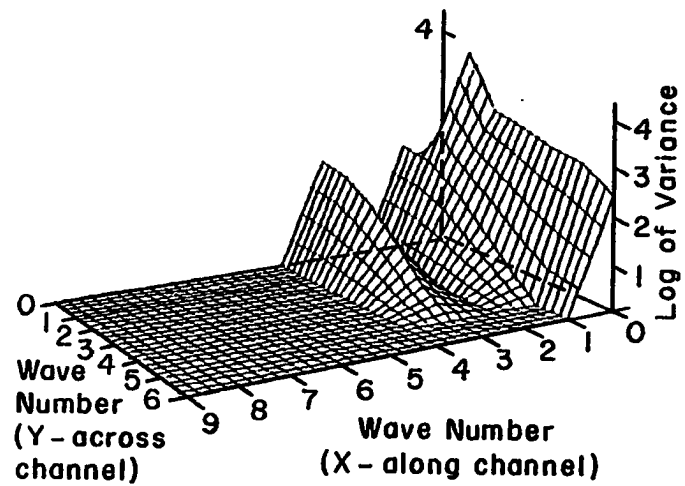
Fig. 6. Fourier analysis of initial height field for shallow water equations

relative amplitudes for the combination of wave numbers in the x (Along the channel) direction and y (across the channel) direction. Basically, the height field slopes from south to north requiring all wave numbers across the channel to be represented. Only wave numbers 1 and 3 are represented along the channel. The amplitudes are plotted on a logrithmic scale so that the smaller amplitudes will be visible.

CHAPTER IV

RESULTS

As described earlier, the three models used were

    1.   Vorticity - Stream Function,

    2.   Penalty Method, and

    3.   Shallow Water Equations.

The tests performed using these models answer the questions relating to element choice, selection of time differencing scheme, and use of lumped or consistent mass. Here the test results are presented for each of the models. Following in Chapter V will be a discussion of the conclusions which may be drawn from these test results taken as a whole.

Vorticity - Stream Function Model

Table 1 shows the results for the comparison of the five elements tested using Crank-Nicholson time differencing and consistent mass. The elements are compared as to position of the nonlinear terms, convergence rate, program size, computer time, and accuracy. The use of (27) with the nonlinear terms on the left side or (28) where they are on the right makes no difference in the accuracy. For each element, this

Table 1. Comparison of 5 Finite Elements using Crank-Nicholson Time-Difference with Consistent Mass.

Number Nodes in Element	Non-linear Terms L≡Left Side R≡Right Side	Average Iteration Per Time Step	Program Size (K Bytes) Fortran H	CPU Time (min) 120 Hr Forecast	RMS Error	
					Stream Function	Vorticity
4	R	3	99.8	2:31	1.2	1.4
4	L	3	112.8	7:04	1.2	1.4
3	R	3	105.2	2:51	1.6	2.0
3	L	3	118.0	7:12	1.6	2.0
6	R	4	135.5	4:29	5.3	8.8
6	L	3	149.6	13:39	5.2	8.8
8	R	4	103.9	3:48	7.2	11.2
8	L	3	119.9	9:05	7.1	11.2
9	R	4	132.5	4:31	2.1	3.2
9	L	3	142.7	14:05	2.0	3.1

result is the same. However, the computer time required when the non-linear terms are on the left is nearly three times as great. In addition, there is a savings of computer storage when the nonlinear terms are on the right side. The only drawback to moving the nonlinear terms to the right side is the slight increase in the average number of iterations required for convergence on each time step in the quadratic elements.

Fig. 7 shows the fields after 120 hours of forecast for the four-and three-node element using consistent mass. The analytic solution is presented for comparison. Fig. 8 gives the same information for the six-and nine-node elements. All of the elements give reasonable solutions; however, the four-node result is clearly the best. The phase speed for the three-and four-node elements is very accurate but the amplitude is reduced slightly more in the three-node than the four-node solution. The nine-node solution has a phase speed which is too small while the six-node solution has phase speed which is slightly high. Both methods result in some distortion of the field with the presence of noise evident in the six-node vorticity field. The results from the eight-node element (not pictured) are very poor. The visual comparisons are supported by the RMSE given in Table 1. Not only is the RMSE the lowest for the four-node element but the program size and computer time are also smaller.
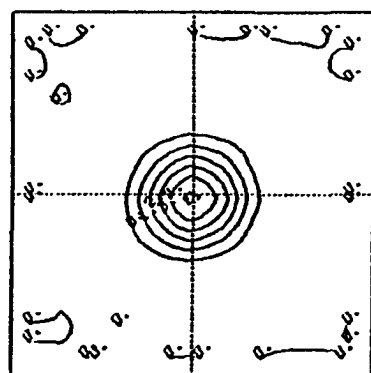
VORTICITY (S⁻¹)   VORTICITY (S⁻¹)   VORTICITY (S⁻¹)
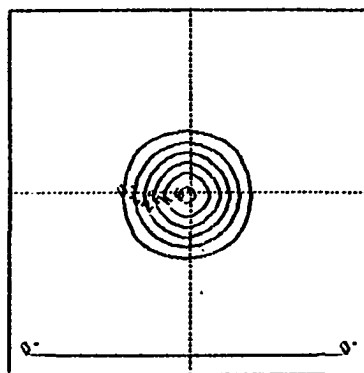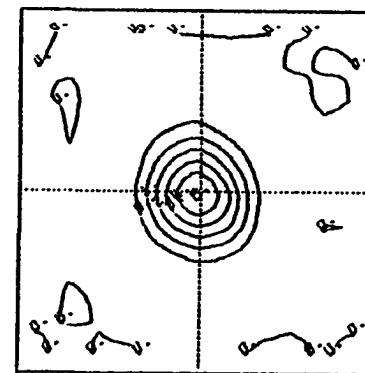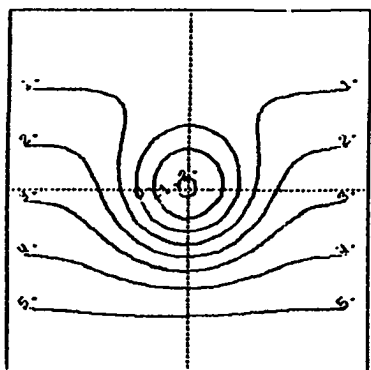
STREAM FUNCTION (M²/S)   STREAM FUNCTION (M²/S)   STREAM FUNCTION (M²/S)
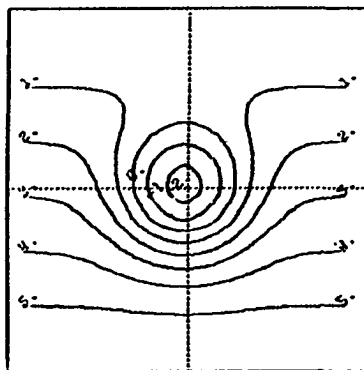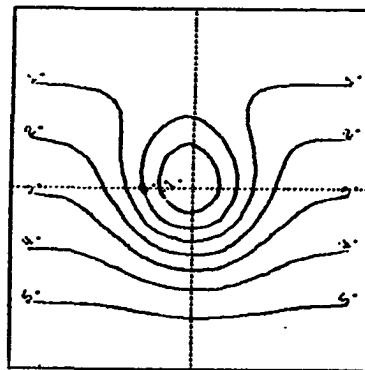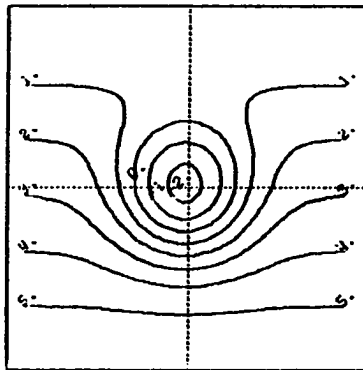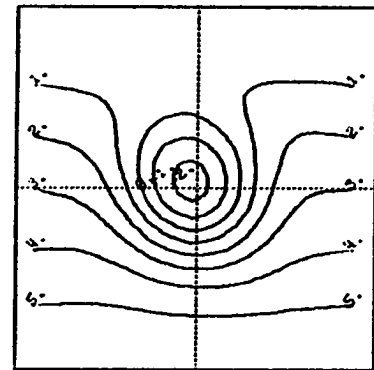
4-Node FEM   Analytic Solution   3-Node FEM

(slant 4)

Fig. 7. Comparison of 4-and 3-node finite elements with Crank-Nicholson time difference and consistent mass after 120 hours for the vorticity-stream function model.
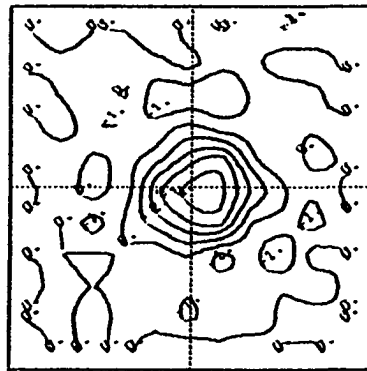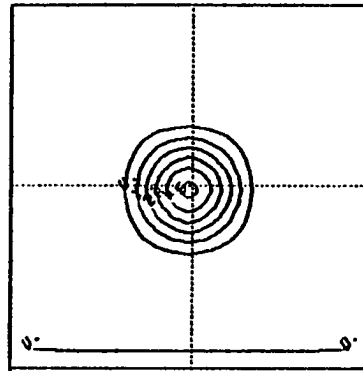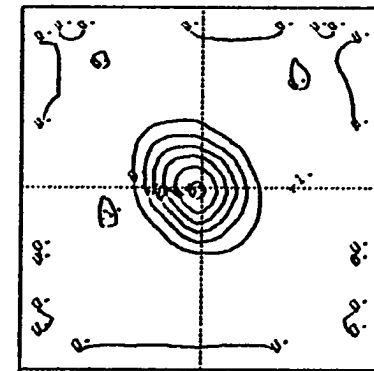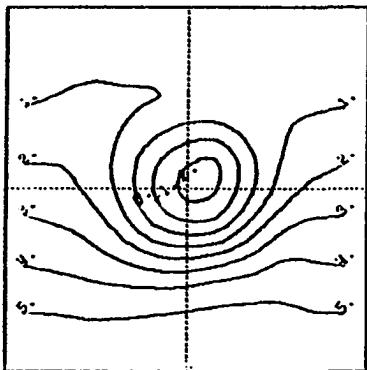
| 6-Node FEM | Analytic Solution | 9-Node FEM |

Fig. 8. Comparison of 6-and 9-node finite elements with Crank-Nicholson time difference and consistent mass after 120 hours for the vorticity-stream function model.

As discussed in Chapter III there are several possible configurations of both the three-and six-node elements when the nodal spacing is held constant. The triangular arrangement chosen does effect the solution. Table 2 gives the RMSE for each of the five configurations (shown in Fig. 5) tested for both the three-and six-node triangular elements. For both elements, the case in which the triangular slant alternates in the direction of flow gives the lowest RMSE. A visual examination of the 120-hour forecast for the three-node element (Fig. 9a-d) reveals little difference in the fields. The vorticity pattern in Fig. 9a,b is slightly distorted in the direction opposite to the constant diagonal slant but this distortion is not evident in the six-node element (Fig. 10a-d). In the six-node element the case which has constant diagonal slant from lower left to upper right (Fig. 10a) has the most accurate phase speed and its RMSE is not significantly different from Fig. 10d which has alternating slant in the direction of flow. It is evident that the linear triangle handles the advection much more accurately than the quadratic regardless of the triangle orientation. The diagonal slant is examined further for the three-node element using the shallow water equations.

Table 1 is based on the use of the consistent mass matrix with Crank-Nicholson time differencing. In contrast, Table 3 contains the same comparison of elements for the lumped or diagonalized mass matrix. The RMSE is considerably

Table 2. Effect of Orientation of Triangular Finite Element within Mesh using Crank-Nicholson Time Differencing Scheme and Consistent Mass for Vorticity-Stream Function Model.

Number of Nodes	Triangle * Orientation	RMS Error	
		Stream Function	Vorticity
3	1	2.7	3.6
	2	2.2	3.4
	3	2.9	6.5
	4	1.6	2.0
	5	3.6	2.4
6	1	5.8	8.2
	2	7.6	12.4
	3	11.1	10.2
	4	5.2	8.8
	5	10.1	8.9

* Diagrams of triangle orientation are given in Fig. 5.

VORTICITY (J⁻¹)   VORTICITY (J⁻¹)   VORTICITY (J⁻¹)   VORTICITY (J⁻¹)

STREAM FUNCTION (M²/S)   STREAM FUNCTION (M²/S)   STREAM FUNCTION (M²/S)   STREAM FUNCTION (M²/S)

a. SLANT 1   b. SLANT 2   c. SLANT 3   d. SLANT 4
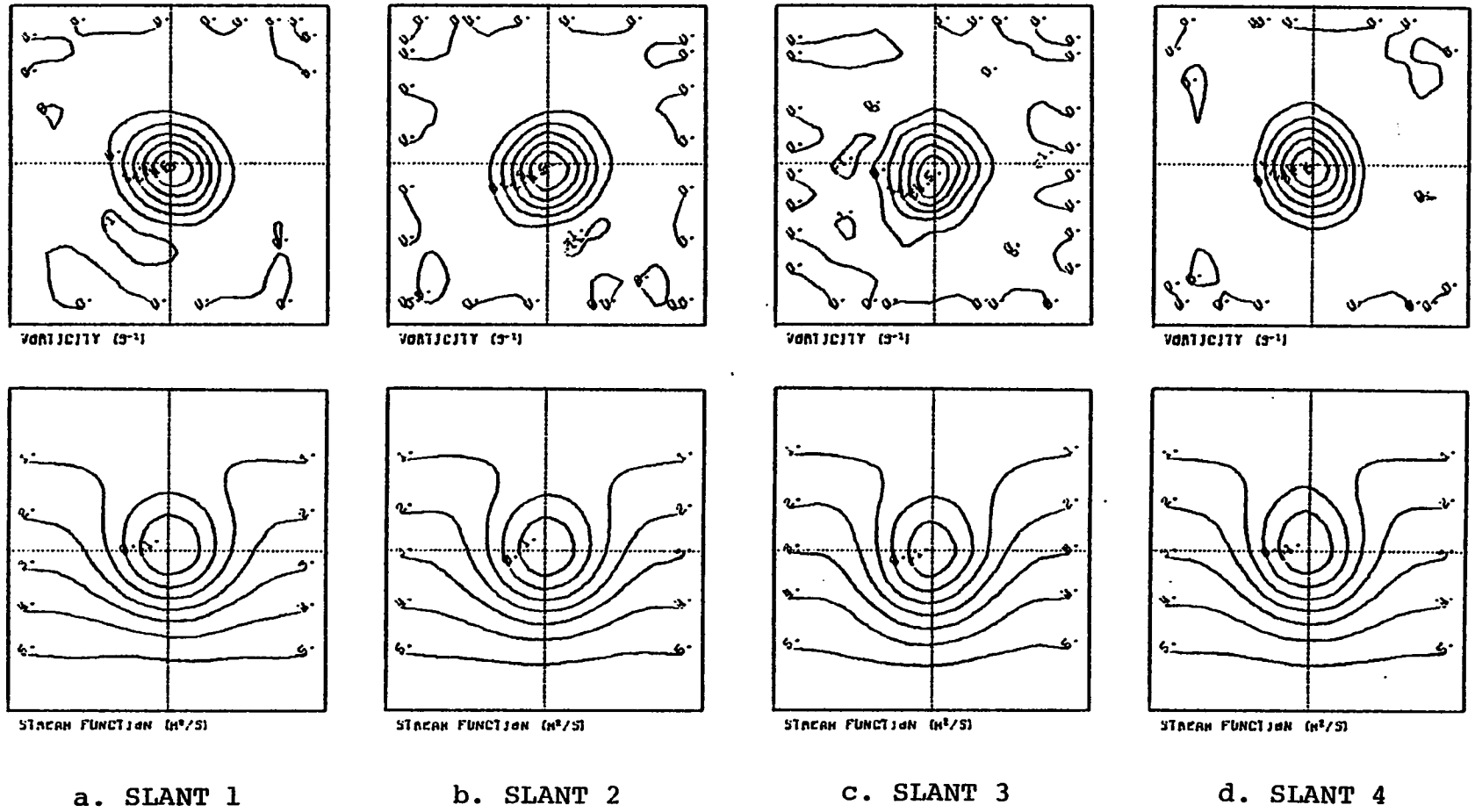
Fig. 9.   120 hour forecast of stream function and vorticity for four different arrangements of 3-node linear triangular element.
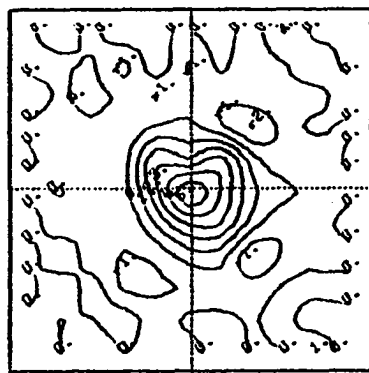
VORTICITY (S⁻¹)　　VORTICITY (S⁻¹)　　VORTICITY (S⁻¹)　　VORTICITY (S⁻¹)
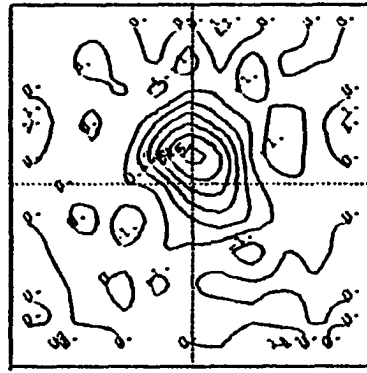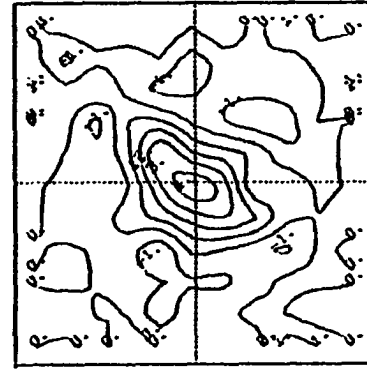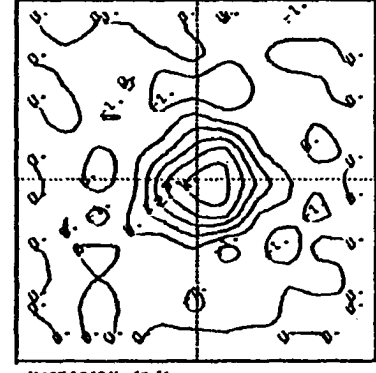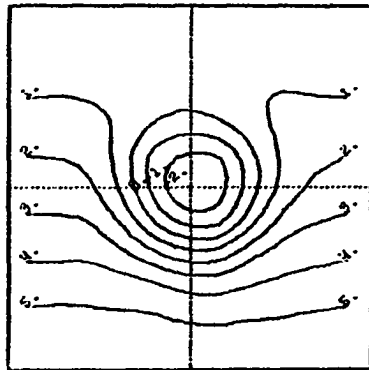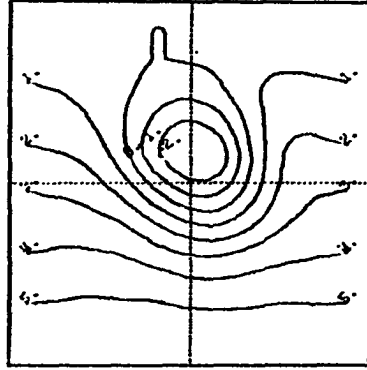
STREAM FUNCTION (M²/S)　STREAM FUNCTION (M²/S)　STREAM FUNCTION (M²/S)　STREAM FUNCTION (M²/S)
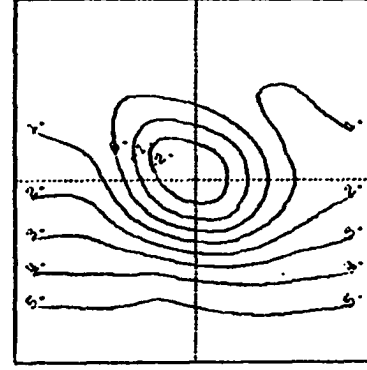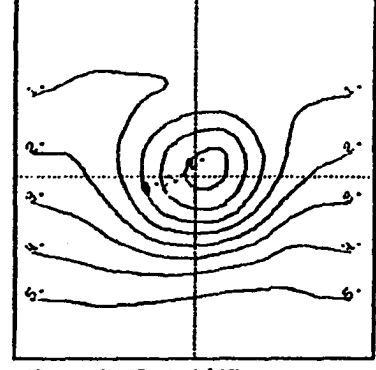
a. SLANT 1　　　b. SLANT 2　　　c. SLANT 3　　　d. SLANT 4

Fig. 10. 120 hour forecast of stream function and vorticity for four different arrangements of 6-node quadratic triangular element.

54

Table 3. Comparison of 5 Finite Elements using Crank-Nicholson Time Difference with Lumped Mass.

Number Nodes in Element	Non-linear Terms L≡Left Side R≡Right Side	Average Iteration Per Time Step	Program Size (K Bytes) Fortran H	CPU Time (min) 120 Hr Forecast	RMS Error	
					Stream Function	Vorticity
4	R	3	88.6	2:30	15.6	19.8
4	L	3	112.8	7:14	15.6	19.8
3	R	3	95.1	2:41	14.6	18.6
3	L	3	118.0	7:05	14.6	18.6
6	R	5	120.5	4:50	12.0	18.1
6	L	3	149.6	14:32	10.4	17.4
9	R	4	118.5	3:44	7.0	9.8
9	L	3	142.7	14:11	7.1	10.0

higher when the mass is lumped, regardless of the element used. Fig. 11 graphically depicts this increase in RMSE for the three-and four-node elements. The phase speed is reasonably accurate but the vorticity center moves southward with considerable loss of amplitude. As shown in Fig. 12, the six- and nine-node elements which use quadratic interpolation provide the better results when the mass is lumped. It is evident in the nine-node element that most of the RMSE is due to inaccuracy in the phase speed.

In summary, the four-node bilinear element has resulted in the most accurate 120-hour forecast. The phase speed and amplitude are close to the analytical solution and the RMSE is the lowest. This element is used to compare five time differencing schemes using both consistent and lumped mass. These results appear in Table 4 (includes comparative information on four-node element repeated from Table 1 and 3). After 120 hours the RMSE for Leap-frog differencing is the same as for Crank-Nicholson. Further, it is difficult to detect any difference between Fig. 13 which shows the Leap-frog result and Fig. 7 which shows the Crank-Nicholson result. The other difference schemes all give reasonably low RMSE. As shown in Figs. 13 and 14, the Matsuno, Galerkin, and Backward methods are all accurate in phase speed but damping of the amplitude accounts for the increased RMSE. Figs. 15 and 16 show 120-hour forecasts for the same time differencing schemes using lumped mass. These lumped mass results do not
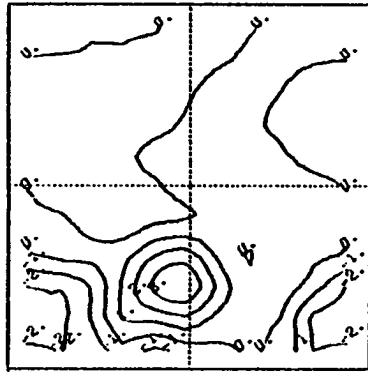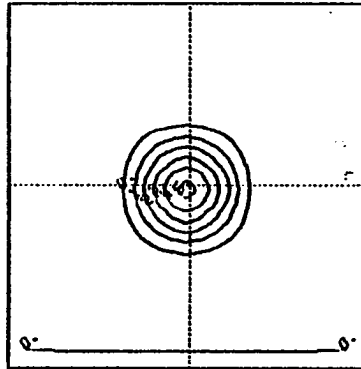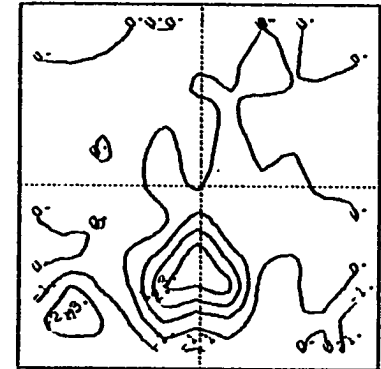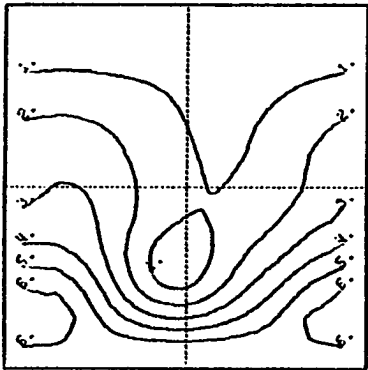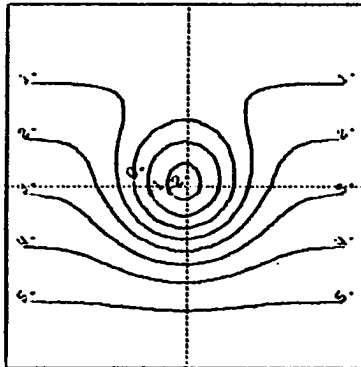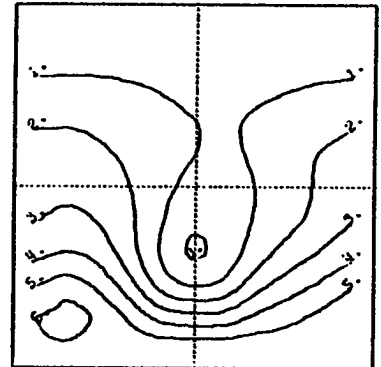
56

VORTICITY (3⁻¹)   VORTICITY (3⁻¹)   VORTICITY (3⁻¹)

STREAM FUNCTION (m²/S)   STREAM FUNCTION (m²/S)   STREAM FUNCTION (m²/S)
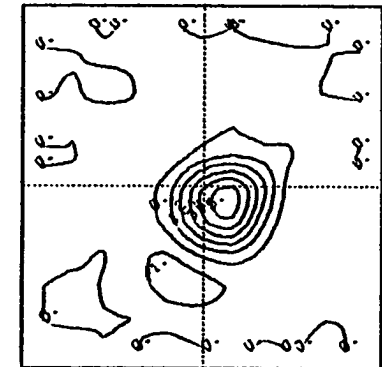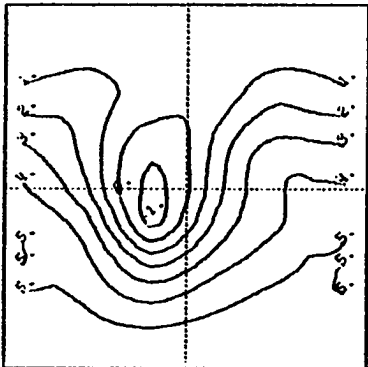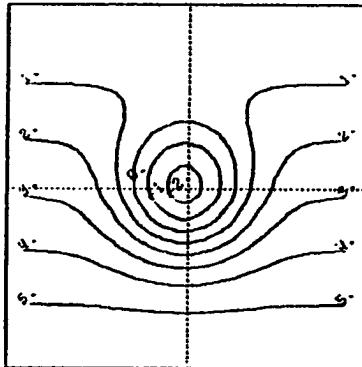
4-Node FEM   Analytic Solution   3-Node FEM

Fig. 11.   Comparison of 4-node and 3-node finite elements with Crank-
Nicholson time difference and lumped mass after 120 hours for the
vorticity stream function model.
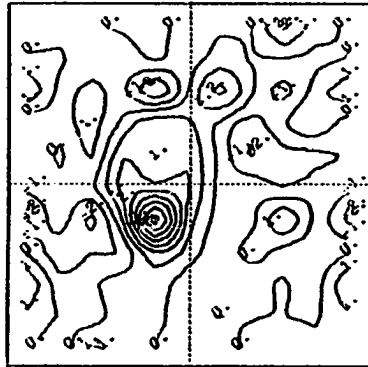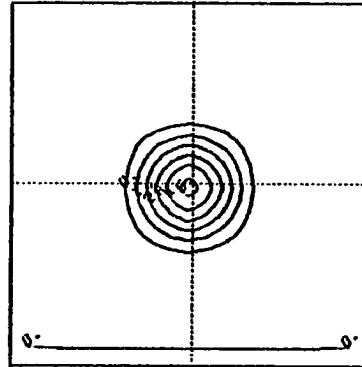
VORTICITY (S⁻¹)   VORTICITY (S⁻¹)   VORTICITY (S⁻¹)

STREAM FUNCTION (m²/s)   STREAM FUNCTION (m²/s)   STREAM FUNCTION (m²/s)
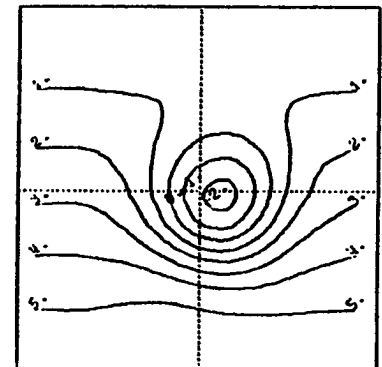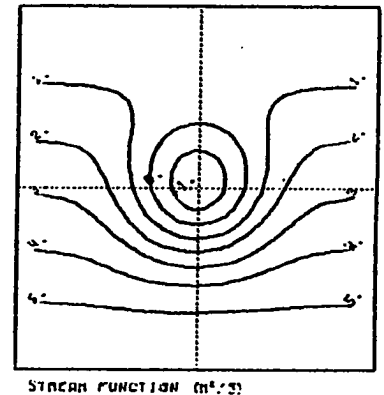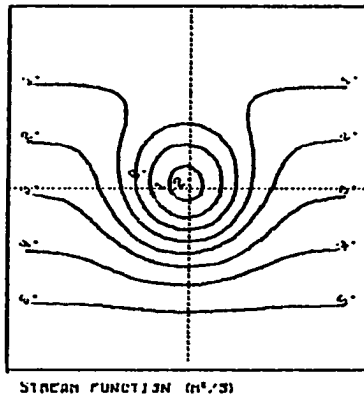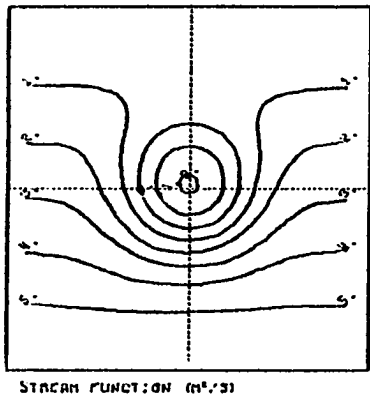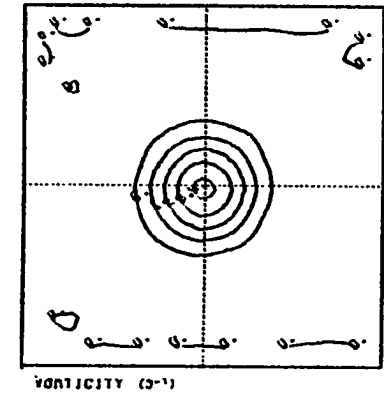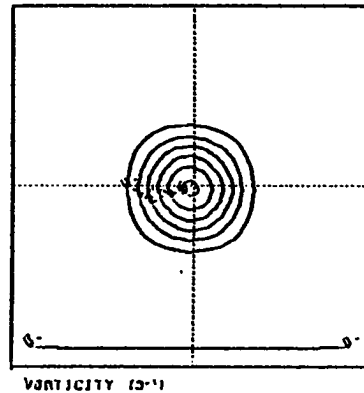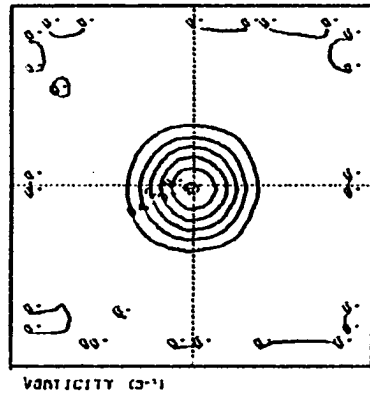
6-Node FEM   Analytic Solution   9-Node FEM

Fig. 12. Comparison of 6-node and 9-node finite elements with Crank-Nicholson time difference and lumped mass after 120 hours for the vorticity-stream function model.

58

Table 4. Comparison of 5 Time-Difference Schemes Using the 4-Node Bilinear Finite Element in Space.

Time Difference Scheme C Consistent L Lumped	Non-Linear Terms L Left Side R Right Side	Average Iteration per Time Step	Program Size (K Bytes) Fortran H	CPU Time (min) 120 hr Forecast	RMS Error	
					Stream Function	Vorticity
Leap Frog -C	Explicit	Explicit	98.4	1:37	1.2	1.4
Leap Frog -L	Explicit	Explicit	98.4	1:30	15.6	19.8
Matsuno -C	Explicit	Explicit	98.2	2:59	2.0	2.3
Matsuno -L	Explicit	Explicit	98.2	3:05	14.4	18.2
Backward -C	R	3	99.7	2:27	3.0	3.9
Backward -C	L	3	112.6	8:13	3.0	3.9
Backward -L	R	3	89.6	2:26	13.6	16.9
Backward -L	L	3	112.5	7:21	13.6	16.9
Galerkin -C	R	3	99.8	2:25	1.7	1.9
Galerkin -C	L	3	112.6	7:26	1.7	1.9
Galerkin -L	R	3	89.6	2:27	14.8	18.7
Galerkin -L	L	3	112.5	7:22	14.8	18.7
Crank-Nicholson -C	R	3	99.8	2:31	1.2	1.4
Crank-Nicholson -C	L	3	112.8	7:04	1.2	1.4
Crank-Nicholson -L	R	3	88.6	2:30	15.6	19.8
Crank-Nicholson -L	L	3	112.8	7:14	15.6	19.8

VORTICITY (3⁻¹)

VORTICITY (3⁻¹)

VORTICITY (3⁻¹)

STREAM FUNCTION (m²/3)

STREAM FUNCTION (m²/3)

STREAM FUNCTION (m²/3)

Leap-frog   Analytic Solution   Matsuno

Fig. 13. Comparison of Leap-frog and Matsuno time differencing with consistent mass after 120 hours using the 4-node finite element for the vorticity-stream function model.

VORTICITY (S⁻¹)

VORTICITY (S⁻¹)

VORTICITY (S⁻¹)

STREAM FUNCTION (M²/S)

STREAM FUNCTION (M²/S)

STREAM FUNCTION (M²/S)

Galerkin

Analytic Solution

Backward

Fig. 14. Comparison of Galerkin and Backward time difference with consistent mass after 120 hours using the 4-node bilinear finite element for the vorticity-stream function model.

VORTICITY (3⁻¹)   VORTICITY (3⁻¹)   VORTICITY (3⁻¹)

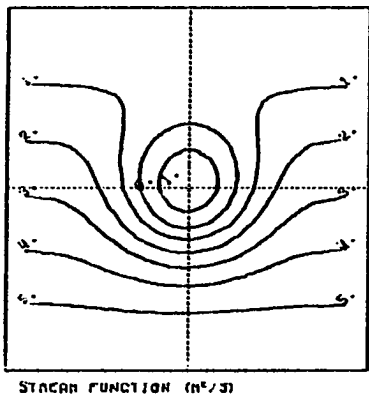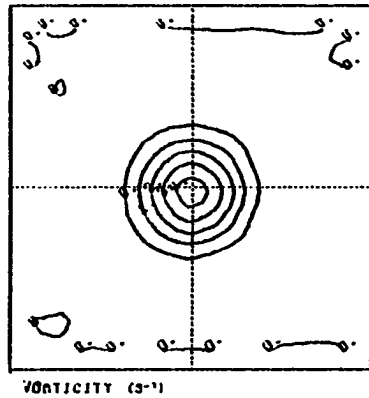STREAM FUNCTION (M²/S)   STREAM FUNCTION (M²/S)   STREAM FUNCTION (M²/S)
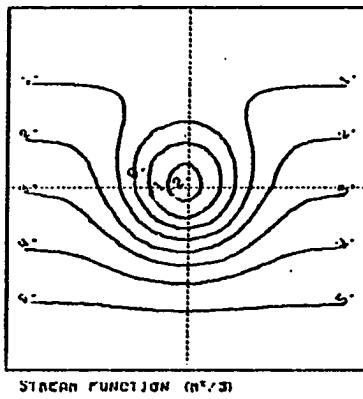
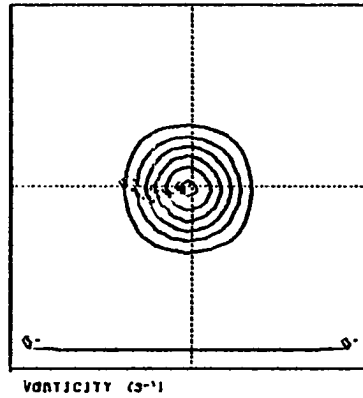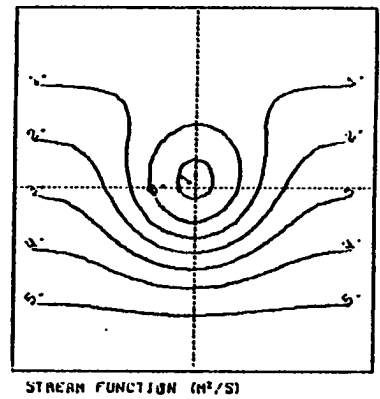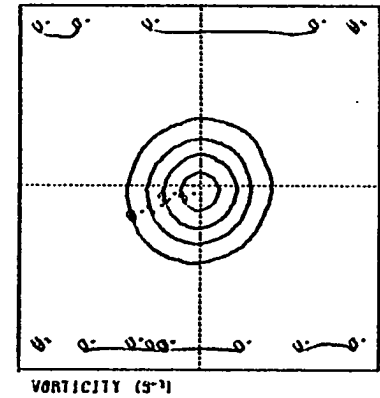Leap-frog   Analytic Solution   Matsuno

62

Fig. 15. Comparison of Leap-frog and Matsuno time differencing with lumped mass after 120 hours using the 4-node finite element for the vorticity-stream function model.

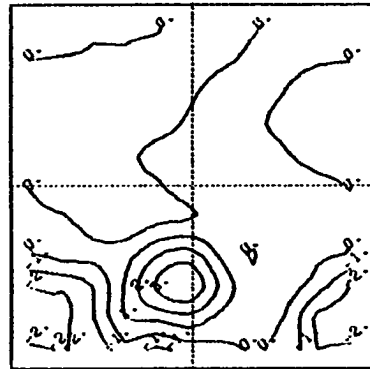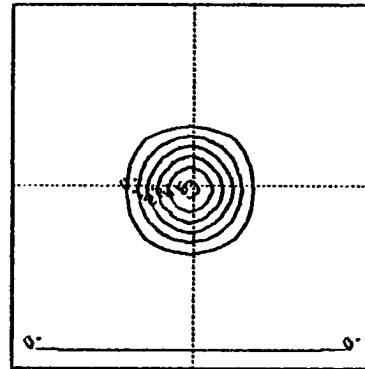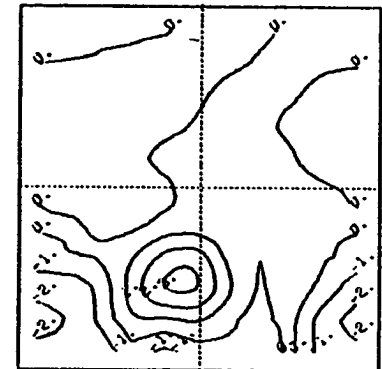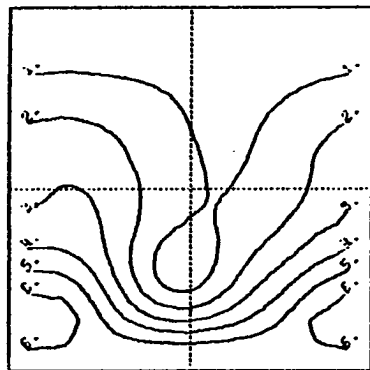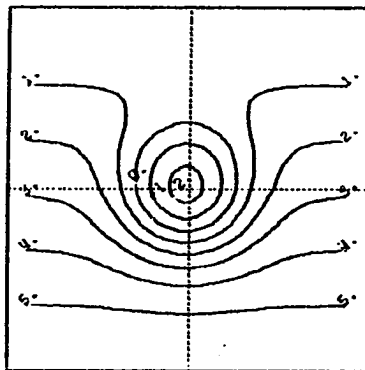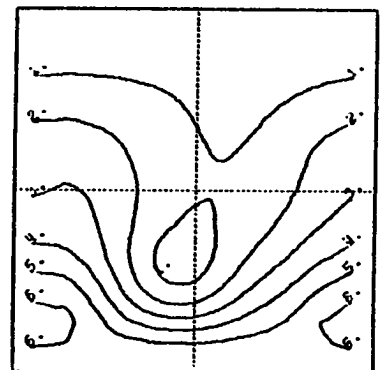Galerkin   Analytic Solution   Backward

Fig. 16. Comparison of Galerkin and Backward time differencing with lumped mass after 120 hours using the 4-node finite element for the vorticity-stream function model.
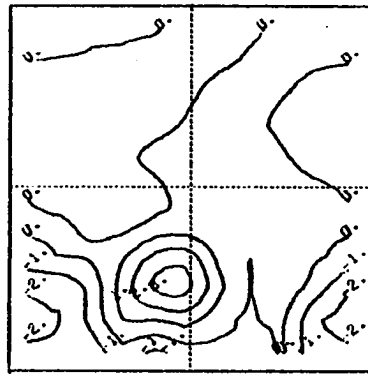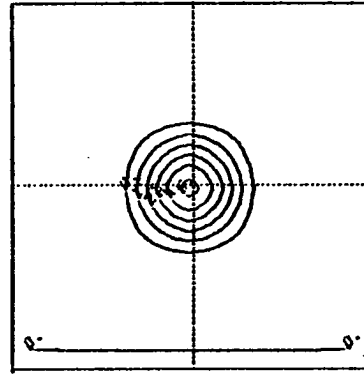
63

differ greatly from the previous discussion nor from the results of Sasaki, and Chang, (1979).

Table 5 gives the results from some finite difference schemes for comparison. The Arakawa difference scheme with consistent mass is given in (21). As stated previously, this scheme is equivalent to the four-node finite element and indeed, the results are the same. The only difference in the two schemes is that no north and south boundary conditions need be specified for vorticity in the FEM but they are necessary to carry out the finite differencing. In this problem, there was no noticeable difference in the result; however, this may not always be the case (Sundstrom, 1973). It should be noted that for a particular problem, when the elements are a regular shape and of equal size everywhere, the FEM can be simplified to a quasi-FD model with corresponding savings in computer time and storage. Here the time requirement decreased three-fold and the storage requirement was half (Table 5). Figs. 17 and 18 show the result for both consistent and lumped mass for Arakawa and centered finite difference methods. The traditional finite difference practitioner would achieve results similar to those with lumped mass. With consistent mass, both the Arakawa and centered difference methods give good results. As shown in Table 5, the use of consistent mass results in approximately a 40 percent increase in computer time over the traditional approach.

Table 5. Results From Finite Difference Methods

Time Difference Scheme C Consistent L Lumped	Space Difference Scheme	Program Size (K Bytes) Fortran H	CPU Time (120 Hour Forecast) (min)	RMS Error	
				Stream Function	Vorticity
Leap Frog-C	Arakawa	46.7	0:28	1.2	1.4
Leap Frog-L	Arakawa	46.7	0:20	16.7	18.8
Leap Frog-C	Centered	46.3	0:27	3.3	5.4
Leap Frog-L	Centered	46.3	0:19	12.8	17.5
Matsuno-C	Arakawa	46.7	0:37	1.8	3.7
Matsuno-L	Arakawa	46.7	0:26	14.0	16.2
Matsuno-C	Centered	46.3	0:39	3.0	5.3
Matsuno-L	Centered	46.3	0:26	10.9	14.5

Table 5. Results From Finite Difference Methods

Time Difference Scheme C Consistent L Lumped	Space Difference Scheme	Program Size (K Bytes) Fortran H	CPU Time (120 Hour Forecast) (min)	RMS Error	
				Stream Function	Vorticity
Leap Frog-C	Arakawa	46.7	0:28	1.2	1.4
Leap Frog-L	Arakawa	46.7	0:20	16.7	18.8
Leap Frog-C	Centered	46.3	0:27	3.3	5.4
Leap Frog-L	Centered	46.3	0:19	12.8	17.5
Matsuno-C	Arakawa	46.7	0:37	1.8	3.7
Matsuno-L	Arakawa	46.7	0:26	14.0	16.2
Matsuno-C	Centered	46.3	0:39	3.0	5.3
Matsuno-L	Centered	46.3	0:26	10.9	14.5

VORTICITY (S⁻¹)

VORTICITY (S⁻¹)

VORTICITY (S⁻¹)

STREAM FUNCTION (M²/S)

STREAM FUNCTION (M²/S)
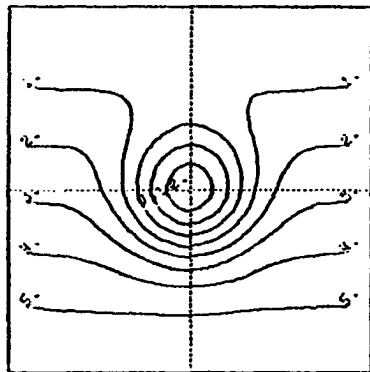
STREAM FUNCTION (M²/S)
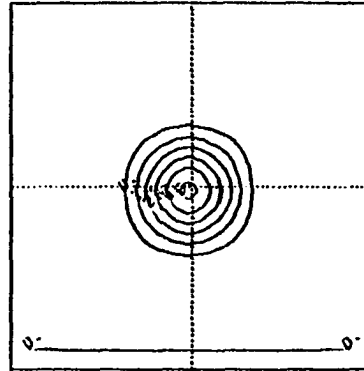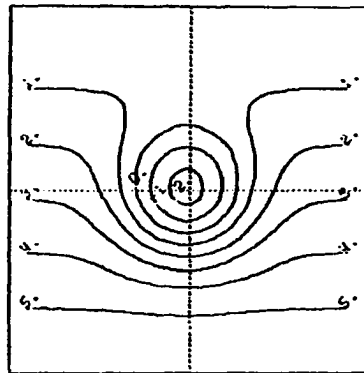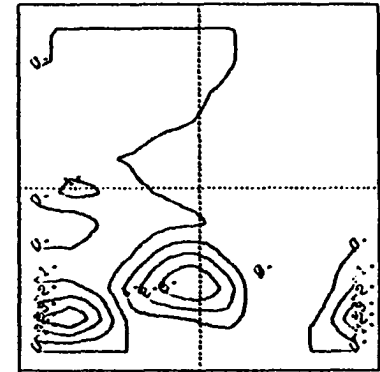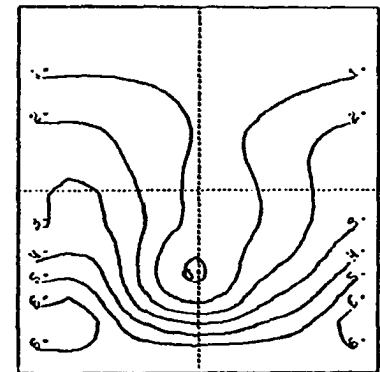
Consistent Mass   Analytic Solution   Lumped Mass
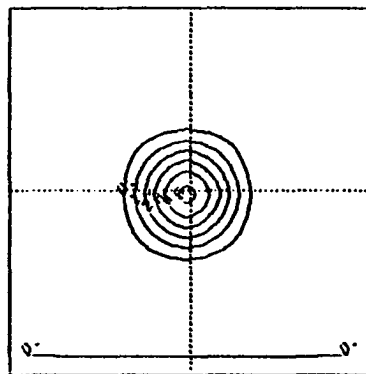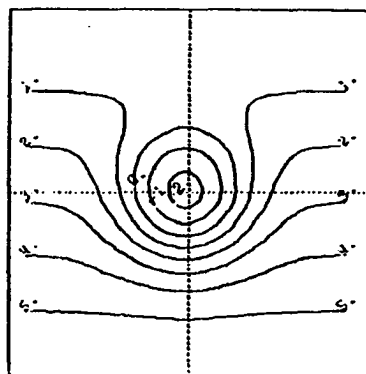
Fig. 17. Leap-frog time difference with Arakawa Jacobian finite difference in space. (vorticity-stream function model)
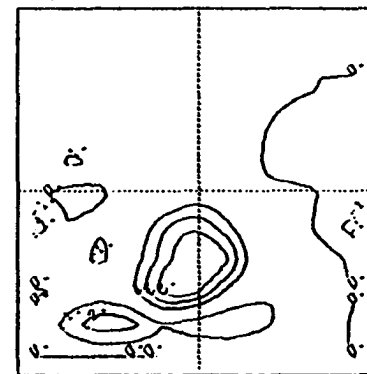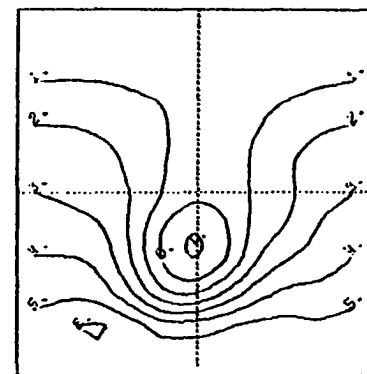
Consistent Mass   Analytic Solution   Lumped Mass

Fig. 18. Leap-frog time difference with centered finite difference in space. (vorticity-stream function model)

Finally, Table 6 shows the results when the three best schemes are intergrated for a longer time using different time steps. As discussed earlier, 1 hour is the upper limit for the Leap-frog integration. Other than the Crank-Nicholson method with 2-hour time step, the result is not significantly different to 240 hours. By 360 hours the Leap-frog scheme is affected by its computational mode but the Crank-Nicholson method allows extremely long integrations. After 1080 hours, the Crank-Nicholson method finally gives a fairly high RMSE; however, this is due mainly to phase speed error. The shape of the fields is quite good.

Penalty-Method

The testing conducted using the penalty method is much less extensive than for the vorticity-stream function model. Table 7 gives the results from comparison of elements using Crank-Nicholson time differencing. The lowest RMSE occurs for the four-node bilinear element. It is followed by the nine-, six-, and eight-node elements. The order is exactly the same as in the previous discussion. Fig. 19 shows the initial and 120-hour forecast for the u and v wind components as well as the stream function and vorticity calculated from the forecast winds. The slight loss of symmetry in the forecast u and v fields indicates that the divergence free condition is not exactly satisfied. In addition, the model has given a reduction in the gradients of u and v which re-

Table 6. Comparison of Three Best Schemes Listed in Tables 1 and 2 with Runs at Different Time Steps.

Scheme: Time Step	Leap Frog Arakawa FD Consistent Mass				Leap Frog 4-node FEM Consistent Mass				Crank-Nicholson 4-node FEM Consistent Mass					
Time Step (hr)	$\frac{1}{2}$		1		$\frac{1}{2}$		1		$\frac{1}{2}$		1		2	
Forecast Time (hr)	RMSE		RMSE		RMSE		RMSE		RMSE		RMSE		RMSE	
	ψ	ζ	ψ	ζ	ψ	ζ	ψ	ζ	ψ	ζ	ψ	ζ	ψ	ζ
120	1.2	1.4	1.2	1.4	1.2	1.4	1.2	1.4	1.2	1.4	1.2	1.4	1.3	1.5
240	2.2	2.6	2.0	2.5	1.8	2.3	1.7	2.3	1.9	2.3	1.9	2.4	2.3	3.0
360	2.8	3.5	2.9	3.4	2.1	2.9	3.8	6.4	2.4	2.9	2.6	3.2	3.3	4.1
480	4.0	5.3	*						2.8	3.2	3.2	3.8	3.9	4.7
600	*										4.5	5.1	5.7	6.6
720											5.8	6.6	7.2	8.4
840											7.6	9.4	8.9	10.4
960											9.4	11.5	11.6	14.3
1080											10.9	13.0	12.6	14.7

Table 7. Penalty Formulation Element Comparison of 120 Hour Forecast

| ELEMENT | RMS ERROR | | CPU TIME (min) |
	VORTICITY	STREAM FUNCTION	
4 node	4.8	2.6	47:07
6 node	10.6	11.4	91:04
8 node	8.5	11.6	58:48
9 node	6.7	6.3	102:02
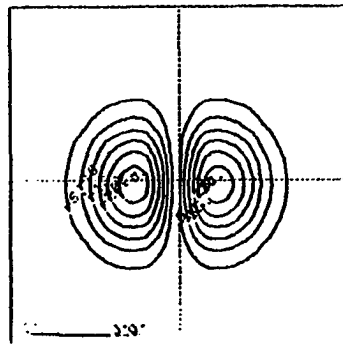
V COMPONENT OF WIND (M/S)
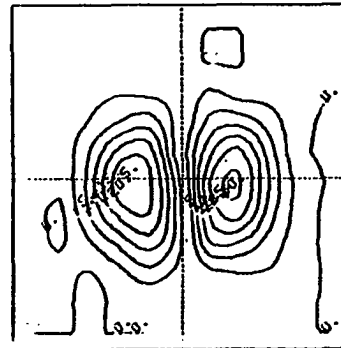
V COMPONENT OF WIND (M/S)
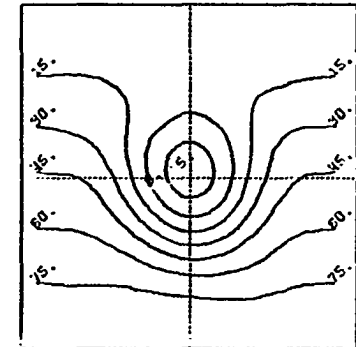
STREAM FUNCTION (M²/S)
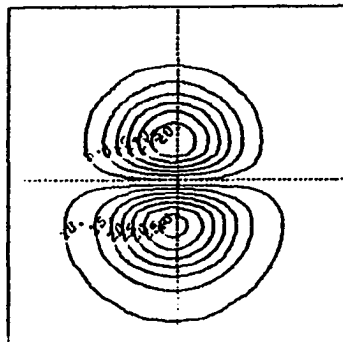
U COMPONENT OF WIND (M/S)
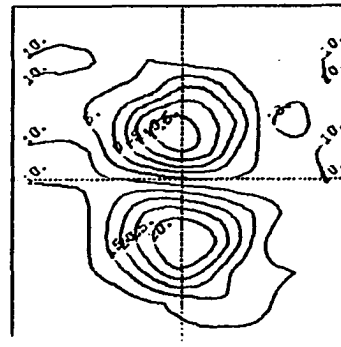
U COMPONENT OF WIND (M/S)
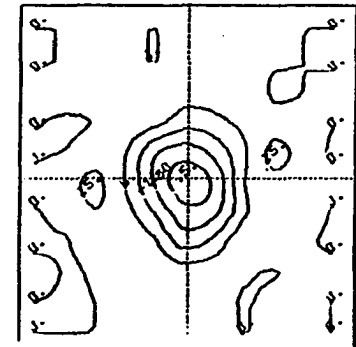
VORTICITY (S⁻¹)

Fig. 19. Initial velocity fields and 120 hour forecast velocity, stream function and vorticity fields using the penalty method.

sults in a decrease in the strength of the vorticity center. The phase speed is as accurate as it was in the vorticity-stream function model but there is a slight northward shift in the vorticity pattern which was not present in the vorticity-stream function model when the four-node element was used (Fig. 7). From Table 6, it is evident that overall, the penalty method is not as accurate for this advection-dominated flow situation as the vorticity-stream function model.

As discussed in Chapter III, approximate values for the pressure may be calculated using (14). The calculated pressure depends not only on the accurate calculation of divergence but also on the proper selection of the penalty parameter λ. This parameter can be found through trial and error. As discussed by Reddy (1979b), too large a value of λ results in the degeneration of the governing equations into only the continuity equation; too small a value means that the continuity equation will not be satisfied. Even when the best value for λ is found, the continuity equation is not exactly satisfied. The resulting pressure values are, at best, an approximation.

The benefit from the use of the penalty method is the reduction of the number of unknowns, thereby reducing the number of equations to two. The form of the equations given by (17) is the traditional approach taken in the application of the FEM. The computational times given in Table 6 using that approach are very long when one considers that the grid

only contains 11 x 11 points. Several attempts have been
made to improve the computation time, such as moving the
nonlinear terms and the penalty term to the force vector, and
separating the u and v equations in order to reduce the order
of the system of linear equations which must be solved.
Every such test resulted in reduced accuracy.

It is because of the inaccuracies in the pressure and
the expense of computation that the penalty method is not
tested to a greater extent. It is interesting however, that
the different approach taken in the penalty method results in
the same relative accuracy of the elements tested.

Shallow Water Equations

Eqs.(18) used for this model present a challenge for
any type of finite discretization because they allow fast
moving gravity waves. The gravity waves are initially of
much lower amplitude than the long waves but they can grow
and after several time steps they can obscure the features
of interest in the solution. Much effort has been directed
toward the control of gravity waves (e.g. Kwizak and Robert,
1971); however, since the intent of this study is to find the
best finite element discretization, the gravity waves are
allowed to develop without any control so that the discreti-
zation may be found which most efficiently discourages their
growth.

All of the elements previously discussed were tested

except the eight-node serendipity element which was eliminated because of its poor performance with the vorticity-stream function and penalty models. The comparison of run times and program size for the models tested is given in Table 8. The three equations were solved one at a time in each time step and/or iteration (depending on the time difference scheme). As occurred in the vorticity-stream function problem, the quadratic (6 and 9 nodes) elements require much more computer time and storage than the three-and four-node elements. The difference in these statistics between the three-and four-node elements is insignificant. Other than these two comparisons there are no other quantitative comparisons; however, there are qualitative differences in the results produced by the elements.

Fig. 20 shows the 48-hour forecast (144 time steps of 20 minutes each) of the height fields, from the six-and nine-node elements using Crank-Nicholson time differencing. Also shown are the corresponding variance plots from the Fourier analyses of those fields. Initially (Fig. 3) there are three equally spaced troughs in the channel. The western trough is shallow to the north and deeper to the south. The centeral and eastern troughs are sharper and deeper to the north. After 48 hours, the troughs move approximately one-third the channel length to the east. As shown, both the six-and nine-node elements produce roughly the same trough positions. Movement is slightly faster for the nine-node case. It can

Table 8. Computational Parameters from Shallow Water Equations Model.

Time Scheme	Nodes*	Position of Non-linear Terms L ≡ Left Side R ≡ Right Side	Time Step (min)	CPU Time (min)	Program Size (K bytes) Fortran H
Crank-Nicholson	3-(1)**	L	20	105:57	200.3
	4	L	20	109:41	194.5
	6	L	20	160:52	261.4
	9	L	20	202:26	253.8
	3-(1)	R	20	37:14	308.0
	3-(2)	R	20	42:12	308.0
	3-(3)	R	20	42:51	308.0
	3-(4)	R	20	39:30	308.0
	3-(5)	R	20	54:01	308.0
	4	R	20	40:41	293.6
Leap frog	4	Explicit	12	10:01	293.6
Matsuno	4	Explicit	12	21:40	293.6
Galerkin	4	R	20	40:15	293.6
Backward	4	R	20	41:08	293.6

* Based on 48 hour forecast.

** Number in parenthesis indicates triangle orientation (see Fig. 5).
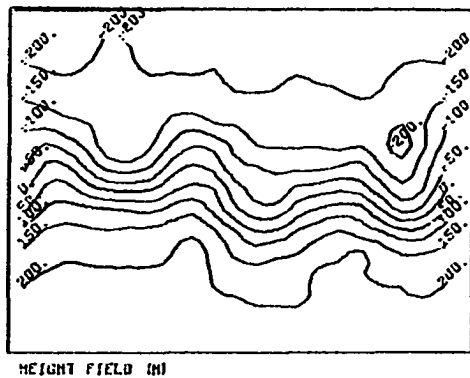
HEIGHT FIELD (M)
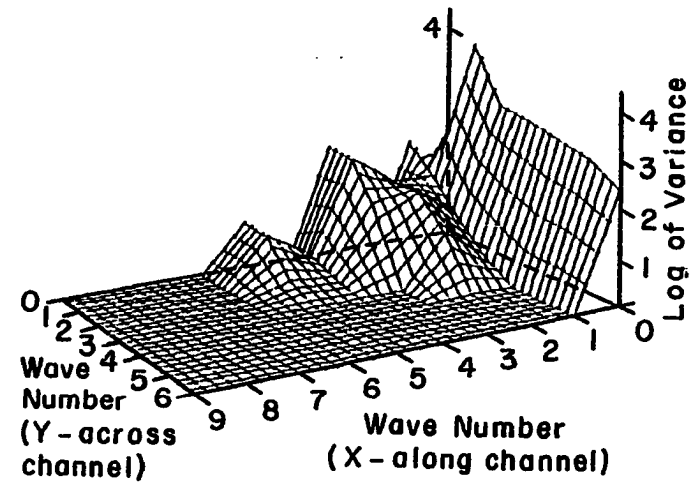
9-Node Element
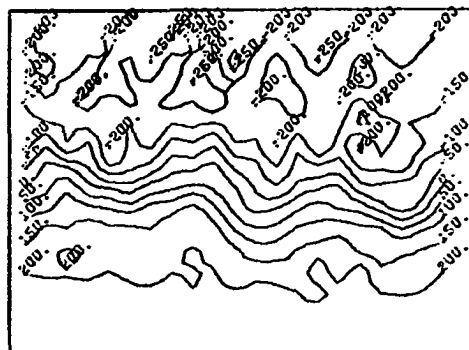
HEIGHT FIELD (M)
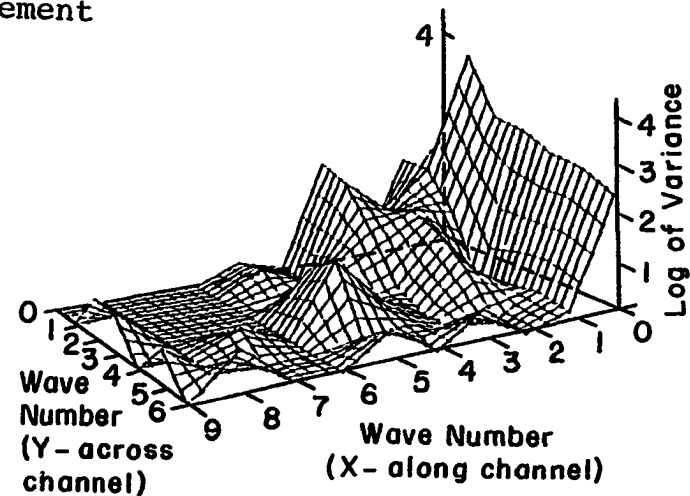
6-Node Element

Fig. 20.   48 hour forecast height field and Fourier analyses for
6-and 9-node elements. (shallow water equations)

readily be seen that the six-node element has resulted in the generation of many short waves at almost every possible wave number, particularly at the highest wave numbers. In contrast, the nine-node element has not led to the production of any short waves. Both elements have produced wave number two and wave number five. This may be a natural consequence of this method since it conserves the average wave number.

Fig. 21 shows the 48 hour height field and its Fourier analysis for the four-node rectangular element using Crank-Nicholson time differencing. The position of the troughs is very close to the nine-node result but the western trough is not as deep as the nine-node case. The Fourier analyses of the nine-and four-node elements are different in two important respects. For the four-node element, the variance at wave number five along the channel is approximately 60 percent of the nine-node result. The same difference is true for the wave associated with wave numbers two and four in the x and y directions respectively. The slightly better result for the four-node element is consistent with the vorticity-stream function and penalty models and is significant when one considers the difference in computational time between the two elements. Some comparable results were also achieved with the three-node element.

The three-node element is used to show the effect of diagonal slant of the triangles. Figs. 22 and 23 show the height fields after 48 hours using Crank-Nicholson time
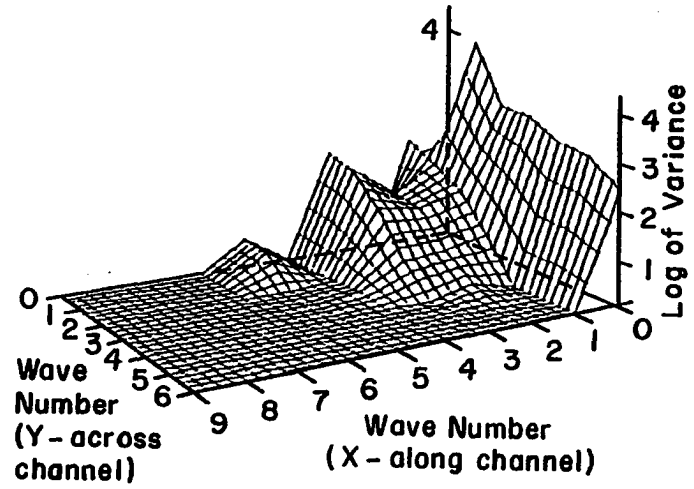
HEIGHT FIELD (M)

Fig. 21.   48 hour forecast height and Fourier analyses for 4-node element.   (shallow water equations)

HEIGHT FIELD (M)

Slant 1

HEIGHT FIELD (M)

Slant 3

HEIGHT FIELD (M)
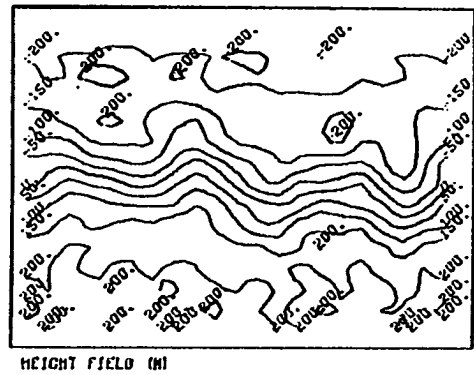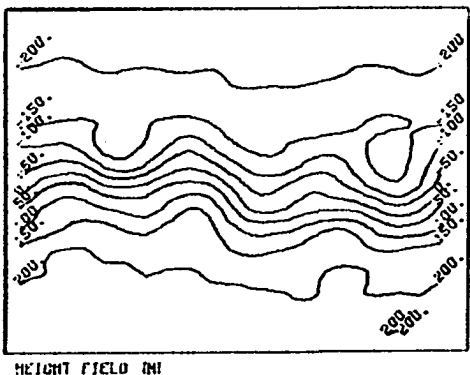
Slant 2
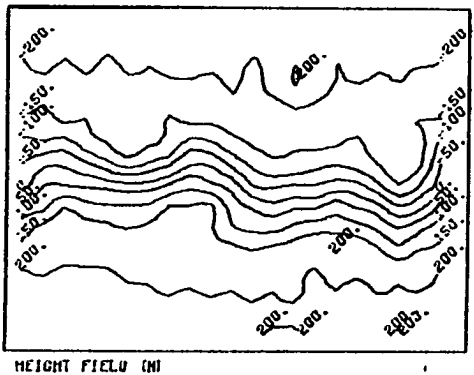
HEIGHT FIELD (M)

Slant 4

Fig. 22.   48 hour forecast height fields for four different arrangements of the linear triangular element.

Slant 1

Log of Variance

Wave
Number
(Y-across
channel)

Wave Number
(X - along channel)

Slant 3

Log of Variance

Wave
Number
(Y-across
channel)

Wave Number
(X - along channel)

Slant 2

Log of Variance

Wave
Number
(Y - across
channel)

Wave Number
(X - along channel)

Slant 4

Log of Variance

Wave
Number
(Y-across
channel)

Wave Number
(X - along channel)
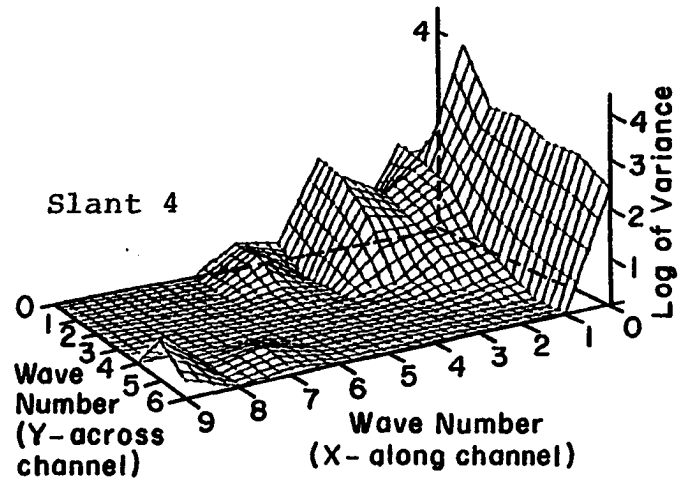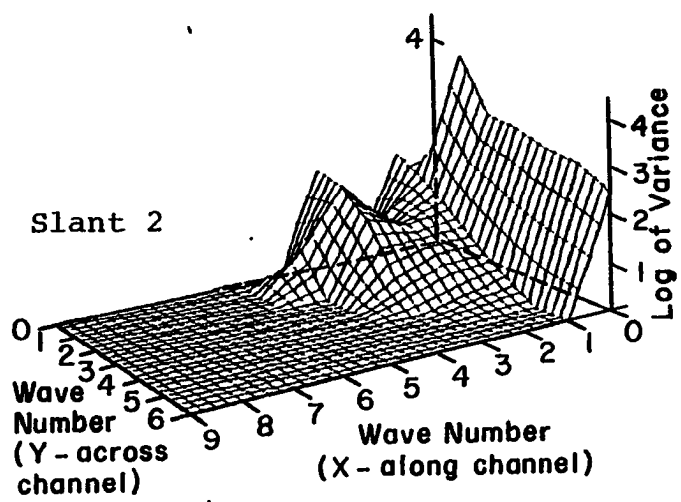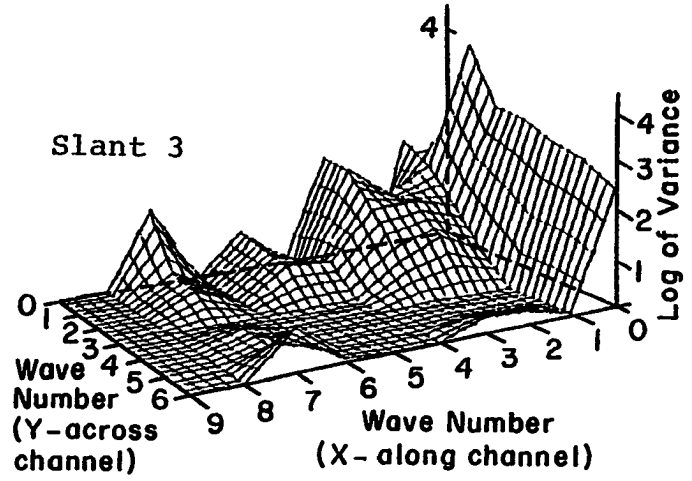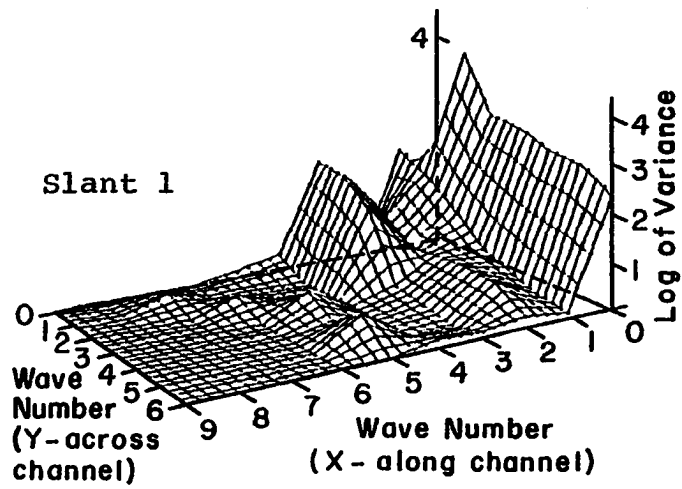
Fig. 23. Fourier analyses of 48 hour forecast height fields for four
different arrangements of the linear triangular element.

differencing for triangle configurations 1-4 (shown in Fig. 5) and the corresponding Fourier analyses. The trough positions are all the same; however, their character differs depending on the triangle slant. For slants 1 and 2, the features tilt slightly in the opposite direction of the constant slant. This is analogous to a distortion found in the vorticity pattern in Fig. 9. The height fields for slants 1 and 2 definitely have a smoother appearance than for slants 3 and 4. This is evident in the Fourier analyses of the fields. The alternating diagonal slant appears to encourage early development of gravity waves. Of these four, the worst case results when the slant alternates across the direction of flow. This is consistent with the vorticity-stream function result for the same triangle orientation. The constant diagonal slant cases appear to give the better results for triangles.

Compared to the four-node element (Fig. 21) the result for slant 2 is almost the same. For slant 2, there is higher variance in the combination of wave number two along the channel and wave numbers four and five across the channel than there is in the four-node case. There is also a development in wave number four along the channel which is not present in the four-node case. Therefore, it appears that the four-node element has slightly better performance in this case.

The four-node element was tested with four other time differencing schemes besides Crank-Nicholson:

1) Galerkin,

2) Backward,

3) Matsuno, and

4) Leap-frog.

As shown in Table 8, all of these schemes were run with the equations formulated so that all terms are in the force vector except the time derivative. Comparing the two four-node Crank-Nicholson cases one can see that this formulation results in a five-fold decrease of computer time. Because no iteration is required, the explicit schemes are much faster.

The results from the Galerkin, Backward, and Matsuno schemes are all similar. All of these schemes cause some damping of the waves. The 48-hour forecast height fields for Matsuno and Galerkin schemes as well as their Fourier analyses are shown in Fig. 24. Compared to the Crank-Nicholson result (Fig. 21) both of these schemes give a smoother forecast field. The only difference in the Fourier analyses is the lower amplitude for wave number five along the channel for both the Galerkin and Matsuno methods compared to the Crank-Nicholson results.

The fastest scheme tested is the Leap-frog or centered time difference. It requires only one-fourth the computation time of Crank-Nicholson and as shown in Fig. 25, it provides reasonable results. At 48 hours, there is more generation of wave number five along the channel as well as higher cross channel wave numbers. The location of the troughs is very
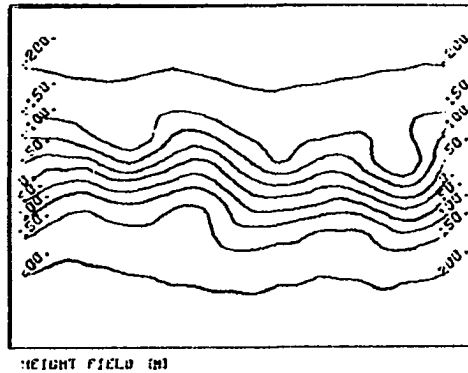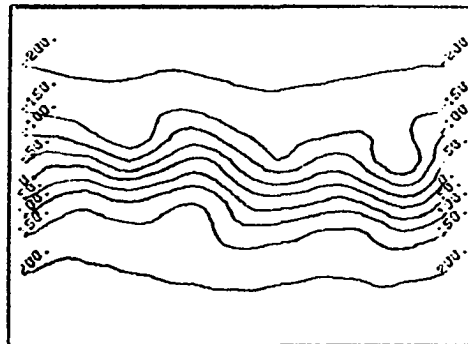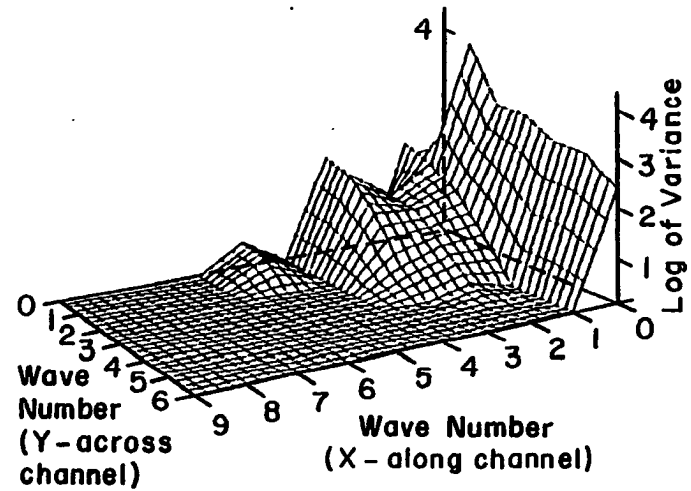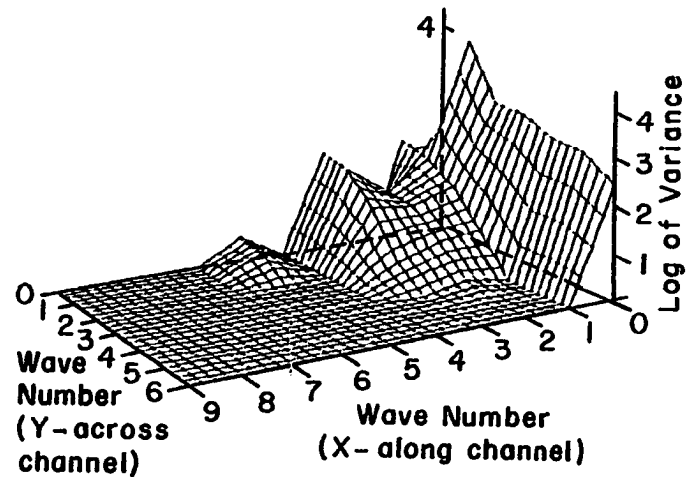
Galerkin

Matsuno
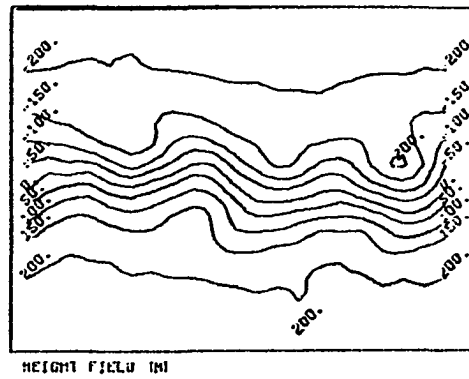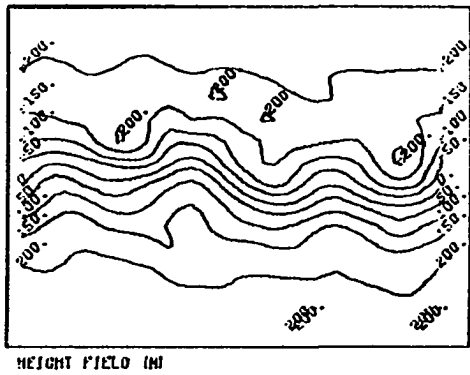
Fig. 24. 48 hour forecast height fields and Fourier analyses from
shallow water equations using Galerkin and Matsuno time differencing.
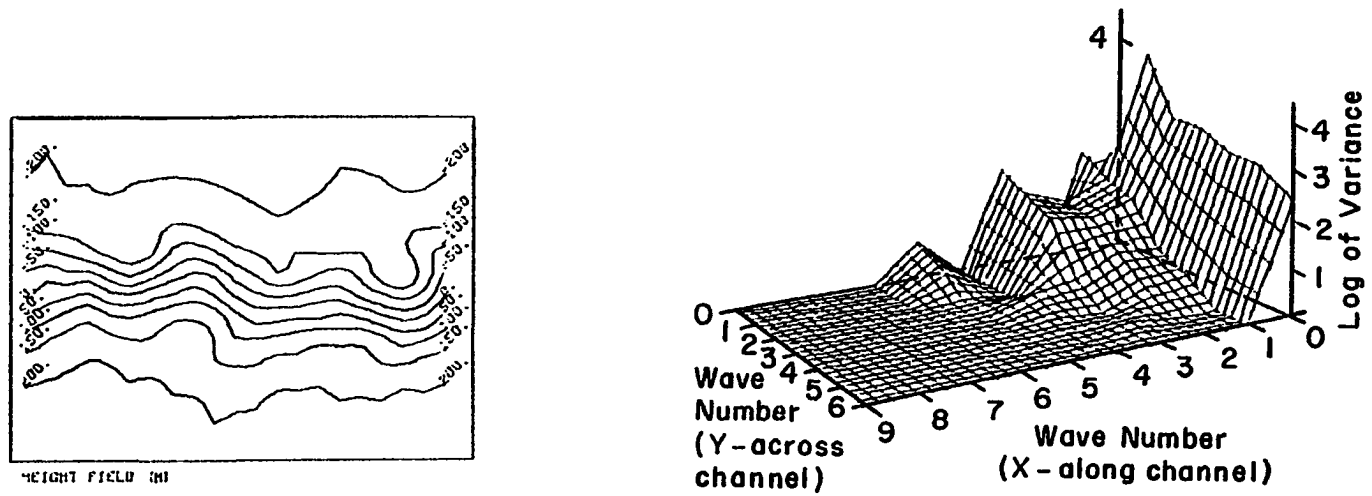
HEIGHT FIELD (M)

Fig. 25.   48 hour forecast height field and Fourier analysis from
shallow water equations using Leap-frog time differencing.

close to the Crank-Nicholson result.

The Leap-frog and Crank-Nicholson schemes are used to demonstrate the conservative properties of the finite element method. As stated earlier, for the shallow water equations, both the total energy and absolute vorticity are conserved. Figs. 26 and 27 show the total energy and vorticity plots for both schemes. As expected, the Leap-frog scheme with its computational mode becomes computationally unstable earlier than Crank-Nicholson. The beginning of instability is evident when one looks at changes in the kinetic energy, a quantity which is not conserved. For the Leap-frog scheme, the kinetic energy increases less than three percent for the first thirty days and then rapidly increases near the thirty-five day mark (see Fig. 28). As shown in Fig. 28, the increase in kinetic energy is much slower for the Crank-Nicholson scheme.
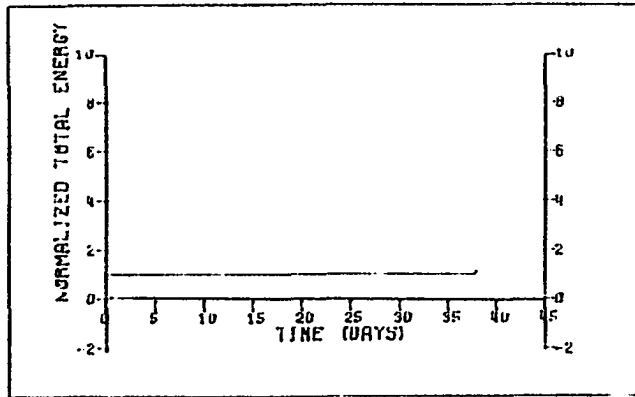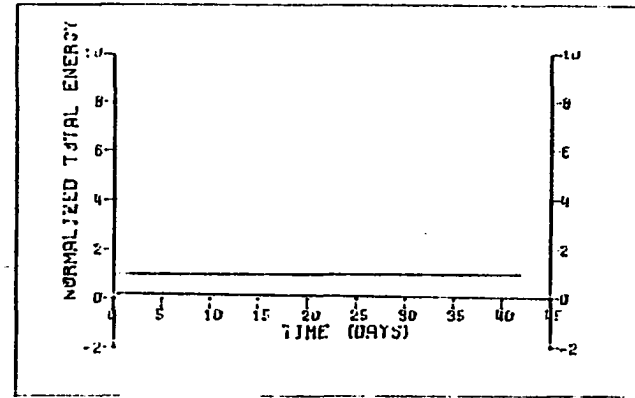
Leap-frog   Crank-Nicholson

Fig. 26. Total energy (normalized) versus time (days)
for Leap-frog and Crank-Nicholson schemes using 4-node
element with shallow water equations.
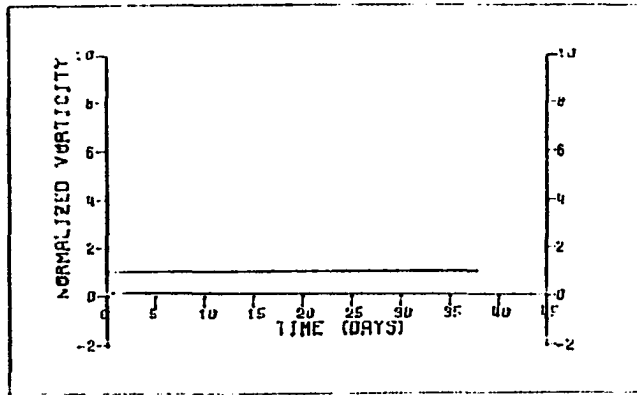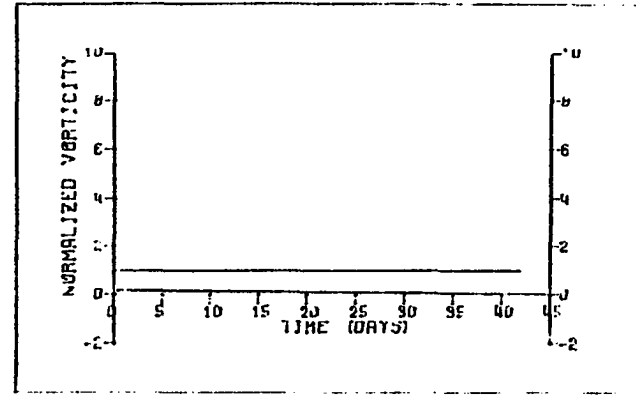
Leap-frog

Crank-Nicholson

Fig. 27. Absolute vorticity (normalized) versus time
(days) for Leap-frog and Crank-Nicholson schemes using
4-node element with shallow water equations.
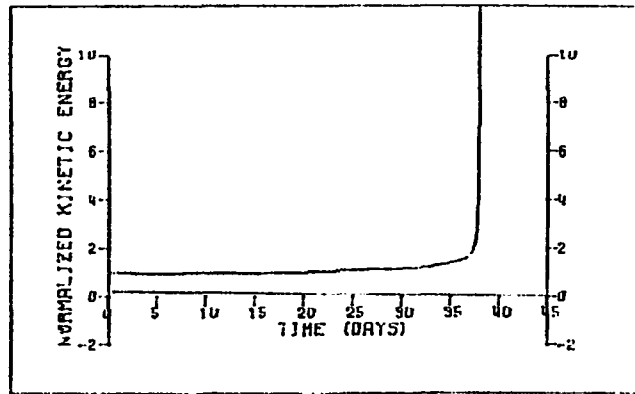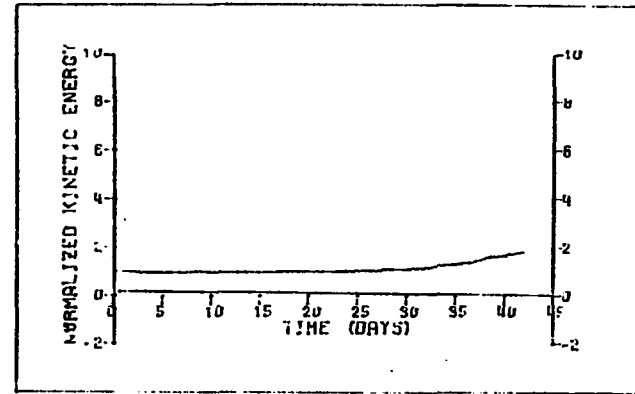
Leap-frog   Crank-Nicholson

Fig. 28. Kinetic energy (normalized) versus time (days)
for Leap-frog and Crank-Nicholson schemes using 4-node
element with shallow water equations.

CHAPTER V

SUMMARY AND CONCLUSIONS

Several tests of the finite element method's ability to handle nonlinear flow problems have been conducted. The investigation has concentrated on spatial discretization, consistent versus lumped mass, time differencing, and computational arrangement of the equations. When combined, the results from the vorticity-stream function, penalty, and shallow water equation models provide consistent answers about the application of the finite element method.

The results from the three models show superior performance when the four-node bilinear element is used. This conclusion is dependent on the total number of nodal or grid points remaining the same. For example, if the nine-node quadratic elements were the same size as the four-node elements there would be a four-fold increase in the total number of grid points and a corresponding increase in computer time; however, the accuracy would be greater than the four-node element of equal size.

Apparently, the key to element accuracy is related to the influence on the solution at a given node by the surround-

ing nodes. Because of the connectivity of the elements, the solution at a node is affected by all the nodes of the elements which share that nodal point. For example, when the mesh consists of four-node elements each nodal point belongs to four elements so that the solution at a given node depends on the eight surrounding nodes. This is true at all interior nodes. In contrast, a mesh made up of nine-node rectangular elements works differently. The corner nodes of the nine-node element are part of four elements so that their solution is affected by the twenty-four surrounding nodes. The mid-side nodes of a nine-node element are part of two elements so that fourteen other nodes affect the solution. And finally, the center node of a nine-node element is only influenced by the other eight nodes in the same element. Other elements have similar relationships. In Fig. 5, it is evident that the triangular element can result in different nodal relationships depending on the element orientation. The worst case occurs for slant 5 where the influence alternates between four and eight surrounding nodes. In a system of equations which allows gravity waves this inconsistent influence of the nodes on each other could enhance the development of gravity waves.

The use of all elements of one size or shape may not always be possible, especially if the finite element method is applied to boundary layer work as planned by Gresho, et al. (1978a) or to models where it is desirable to have a nested fine mesh grid. Further research is required in order to

determine the effects of variable mesh on the solutions. However, this study indicated that the rectangular element should be the primary element used in advective flow models with the triangular element employed only when absolutely necessary to accomodate an irregular boundary. The use of higher order elements is neither economically nor computationally desirable.

This study substantiates the findings of Gresho, Lee, and Sani (1977) regarding consistent and lumped mass. Studying an advective-diffusive model involving dissipation of pollutants they found that the solution suffers when mass lumping is applied. Here and in concert with the related work of Sasaki and Chang (1979), it is clearly shown that regardless of the time differencing scheme used, the accuracy of advective calculations is severely reduced by lumping the mass. Since the mass is inherently lumped in finite difference models the loss of accuracy is normally improved by using a finer grid resolution. As shown by Cullen (1974a), for some problems the finite element method with consistent mass performs as well as a finite difference model with four times the grid resoltuion.

Related to the question of consistent versus lumped mass is the problem of choosing a time difference scheme. Aside from the problem of controlling gravity waves it is apparent that when consistent mass is employed, there is little difference in the solution as long as the time integration is

not carried for a long time. As shown, the Crank-Nicholson scheme allowed long term time integration with only slight changes in the total energy while the Leap-frog scheme allowed faster development of the gravity waves. However, with the four-node element, Leap-frog time differencing is four times faster than Crank-Nicholson. Based on these results, an explicit scheme such as Leap-frog appears to be a good compromise, especially if it is combined with some type of time filter. Other alternatives include the use of the semi-implicit scheme of Kwizak and Robert (1971) as planned in the model under development in Canada (Staniforth and Mitchell, 1978).

The final topic under consideration deals with the computational arrangement of the equations. From an economic standpoint, much can be gained by rearrangement of the equations. Computation time can be drastically reduced in the finite element method by solving the equations for the time rate of change of the variables rather than the variables themselves. By using additional storage, the mass matrix can be preprocessed and stored, saving additional time. If the finite element method is applied to a problem with uniform grid spacing then it is possible to transform it into a quasi-finite difference model thus increasing the computer efficiency. Such a transformation has been made by Jesperson (1974), for the vorticity-stream function model and as shown here, results in a four-fold savings of computer time. Therefore, even

though the finite element method is complicated compared to conventional finite difference methods it can be made very competitive and can result in increased accuracies.

In summary, further research into the application of the finite element method is warranted. In particular, the following topics should be investigated.

1. Because of the potential uses in meteorology, a detailed examination of the effects of grid refinement should be made. Several options such as reduction of the grid through the prudent use of triangular elements, smooth versus abrupt reductions in rectangular element size, and moving fine mesh grids inside coarse mesh grids should be studied.

2. The use of variational constraints as developed by Sasaki (1976) should be investigated. The finite element method naturally conserves certain properties depending on the governing equations; however, as demonstrated by Sasaki using finite difference methods, some improvement can be made through the use of variational constraints.

3. Modelling of the equations on the globe should be studied. Cullen (1974b) used a specialized triangular mesh for this work but did not perform an exhaustive

study. In particular, the finite element method should be able to handle the changing resolution caused by the geometry as well as the singularity points at the north and south poles.

4. The extension of the model to the vertical dimension should be examined. Staniforth and Daley (1979) have begun development of a baroclinic model; however, studies should be made as to the required resolution in the vertical when the FEM is employed.

5. Investigations should be made into the modelling of terrain in a finite element model. Preliminary studies can be made with the shallow water equations in two dimensions by placing an obstruction in the channel. More sophisticated studies should then be made with three dimensional flow and eventually with baroclinic models.

BIBLIOGRAPHY

Arakawa, A., 1966: Computational design for long term numerical integration of the equations of fluid motion: Two-dimensional incompressible flow. Part 1. J. Comput. Phys., 1, 119-143.

Carnahan, B., H.A. Luther, and J.O. Wilks, 1968: Applied Numerical Methods, John Wiley and Sons, New York, 604 pp.

Courant, R., 1943: Variational methods for the solution of problems of equilibrium and vibration. Bull. Am. Math. Soc., 49, 1-23.

Cullen, M.F.P.; 1973: A simple finite element method for meteorological problems. J. Inst. Math. Applics., 11, 15-31.

_____, 1974a: A finite element method for a non-linear initial value problem, J. Inst. Maths. Applics., 13, 233-247.

_____, 1974b: Integration of the primitive equations on a sphere using the finite element method. Quart. J.R. Met. Soc., 100, 555-562.

_____, 1976: On the use of artificial smoothing in Galerkin and finite difference solutions of the primitive equations. Quart. J.R. Met. Soc., 102, 77-93.

Fix, G.J., 1976: Finite element models for ocean circulation problems, SIAM J. Appl. Math., Col. 29, No. 3, 371-387.

Goodman, J.W., 1968: Introduction to Fourier Optics., McGraw-Hill, San Francisco, 287 pp.

Grammeltvedt, A., 1969: A survey of finite-difference schemes for the primitive equations for a barotropic fluid, Mon. Wea. Rev., 97, 384-404.

Gresho, P.M., R.L. Lee, R.L. Stullich, and R.L. Sani, 1978a: Solution of the time-dependent Navier-Stokes equations via FEM, presented at 2nd Int. Conf. on FEM in Water Resources, July 10-14, London, England.

_____, _____, R.L. Sani, and T.W. Stullich, 1978b: On the time dependent FEM solution of the incompressible Navier-Stokes equations in two and three dimensions, presented at 2nd Conf. on FEM in Water Resources, July 10-14, London, England.

_____, _____, T.W. Stullich, and R.L. Sani, 1978c: Solution of the time dependent Navier-Stokes equations via FEM. Preprint UCRL-80125, Lawrence Livermore Laboratory.

_____, _____, and R.L. Sani, 1977: "Advection Dominated Flows with Emphasis on the Consequences of Mass Lumping", to be published in Finite Elements in Fluids, Vol. 3, J. Wiley & Sons.

Haltiner, G.J., 1971: Numerical Weather Prediction, John Wiley & Sons, Inc., New York, 317 pp.

Huebner, K.H., 1975: The Finite Element Method for Engineers, Wiley-Interscience, New York.

Huyakorn, P.S., C. Taylor, R.L. Lee, and P.M. Gresho, 1978: A comparison of various mixed-interpolation finite elements in the velocity-pressure formulation of the Navier-Stokes equations, submitted to Computers and Fluids.

Jespersen, D.C., 1974: Arakawa's method is a finite-element method. J. Comput. Phys., 16, 383-390.

Kawahara, M., 1977: Periodic Galerkin finite element method of unsteady periodic flow of viscous fluid. Int. J. Num. Meth. Eng., 11, 1093-1105.

_____, and K. Hasegawa, 1977: Periodic Galerkin Element method of tidal flow. Int. J. Num. Mech. Eng., (in press).

_____, _____, and Y. Kawanago, 1977: Periodic tidal flow analysis by finite element perturbation method. Computers and Fluids, 5, No. 4, 175-189.

Kelley, Jr., R.G., and R.T. Williams, 1976: A finite element prediction model with variable element sizes, Tech. Rept. NPS-63Wu 76101, Naval Postgraduate School.

Kwizak, M., and A.J. Robert, 1971: A semi-implicit scheme
    for grid point atmospheric models of the primitive
    equations. Mon. Wea. Rev., Vol. 99, No.1, 32-36.

Mesinger, F., and A. Arakawa, 1976: Numerical Methods used
    in Atmospheric Models. WMO/ICSU Joint Organizing
    Committee, CARO Publication Series No.17, 64 pp.

Oden, J.T., 1972: Finite Elements of Nonlinear Continuum,
    McGraw-Hill Book Co. Ltd., New York, 432 pp.

Oden, J.T., and J.N. Reddy, 1976: An Introduction to the
    Mathematical Theory of Finite Elements. John Wiley
    and Sons, New York, 429 pp.

Reddy, J.N., 1979a: "On the Finite Element Method with Pen-
    alty for Incompressible Fluid Flow Problems", Proc.
    Conf. on the Mathematics of Finite Elements and
    Applications, J.R. Whiteman (ed), Academic Press,
    New York, 1979, 227-235.

_____, 1979b: "Penalty Finite Element Methods for the Solu-
    tion of Advection and Free Convection Flows",Finite
    Element Methods in Engineering ed by A.P. Kabila and
    V.A. Pulmano, 583-598.

Sadourny, R., 1973: Forced geostrophic adjustment in large
    scale flows. Unpublished manuscript, Laboratoire de
    Meteorologie Dynamique du DNRS, 92-- Meudon-Bellevue,
    France.

Sasaki, Y.K. 1970a: Numerical variational analysis formulated
    under the constraints as determined by longwave equa-
    tions and a low-pass filter. Mon. Wea. Rev., 98,
    #12, 884-899.

_____, 1970b: Numerical variational analysis with weak con-
    straint and application to surface analysis of sev-
    ere storm gust. Mon. Wea. Rev., 98, #12, 900-912.

_____, 1976: Variational design of finite difference schemes
    for initial value problem with an integral invariant.
    J. Comp. Physics, 21, 270-278.

_____, and J.N. Reddy, 1979: "A Comparison of Stability and
    Accuracy of Some Numerical Models of Two-Dimensional
    Circulation", Second Int. Conf. Computational Methods
    in Nonlinear Mechanics, The Univ. of Texas at Austin,
    TX, March 26-29, also to appear in Int.J.Numer. Meth.
    Engng.

_____, and T. Chang, 1979: A comparison of numerical schemes
    for two dimensional vorticity equation. (Manuscript
    in preparation).

Segerlind, 1976: Applied Finite Element Analysis. J. Wiley & Sons, New York.

Staniforth, A.N., and H. Mitchell, 1977a: A semi-implicit finite element barotropic model. Mon. Wea. Rev., 105, 154-169.

_____, and R.W. Daley, 1977b: A finite-element formulation for the vertical discretization of sigma coordinate primitive equation models. Mon. Wea. Rev., 105, 1108-1116.

_____, and H. Mitchell, 1978: A variable-resolution finite-element model for regional forecasting with the primitive equations. Mon. Wea. Rev., 106, 439-447.

_____, and R.W. Daley, 1979: A baroclinic finite element model for regional forecasting with the primitive equations, Mon. Wea. Rev., 107, 107-121.

Strang, A., and G. Fix, 1973: An Analysis of the Finite-Element Method. Prentice Hall, 306 pp.

Sundstrom, A., 1973: Theoretical and Practical Problems in Formulating Boundary Conditions for a Limited-Area Model. Report DM-9, International Meteorological Institute in Stockholm.

Zienkiewicz, O.C., 1977: The Finite Element Method, 3rd ed., McGraw-Hill Book Co. Ltd., New York, 787 pp.

APPENDIX A

THE FINITE ELEMENT METHOD

Introduction

The purpose of this appendix is to provide a capsule description of some of the pertinent details about the finite element method. Topics discussed are the Galerkin method, discretization of the domain, and development of interpolation functions. Additional details may be found in Segerlind (1976), Strang and Fix (1973), Oden and Reddy (1976), and Zienkiewicz (1977).

Galerkin Method

The Galerkin method is a variational method which can be applied to linear as well as nonlinear problems because there is no requirement that the functional be known.

Suppose the following governing equation is specified

$$-\nabla^2 u = f \text{ in } \Omega, \quad u = 0 \text{ on } \partial\Omega \tag{A1}$$

The solution, $u(x,y)$ is approximated by

$$u(x,y) \simeq u_e(x,y) = \sum_{i=1}^{N} u_i N_i(x,y) \tag{A2}$$

where N_i are approximating functions which satisfy some continuity requirements as well as the boundary conditions. If the approximation (A2) is substituted into the governing equation (A1) the result is

$$-\nabla^2 u_e - f = R(x,y) \tag{A3}$$

where $R(x,y)$ is the error of the approximation. The Galerkin method minimizes this error as follows

$$\iint_\Omega R(x,y) \, N_i(x,y) \, dxdy = 0, \tag{A4}$$

$$\text{or} \quad \iint_\Omega (-\nabla^2 u_e - f) N_i(x,y) \, dxdy = 0. \tag{A5}$$

So, the error is made orthogonal to the set of approximating functions. Substituting u_e into (A5) gives

$$\sum_j \iint_\Omega (-\nabla^2 N_j(x,y)) N_i \, dxdy \, u_j = \iint_\Omega f \, N_i(x,y) dxdy. \tag{A6}$$

The left side of (A6) can be transformed using the product rule of differentiation and Green's theorem giving

$$\sum_j \iint_\Omega \left(\frac{\partial N_i}{\partial x} \frac{\partial N_j}{\partial x} + \frac{\partial N_i}{\partial y} \frac{\partial N_j}{\partial y} \right) dxdy \, u_j = \iint_\Omega f \, N_i(x,y) dxdy$$

$$+ \oint_{\partial\Omega} (u_e N_i n_x + u_e N_i n_y) \, ds, \tag{A7}$$

where (n_x, n_y) are the unit normal vectors to the boundary $\partial\Omega$. Since u is specified (A1) on $\partial\Omega$ the boundary term is zero and may be dropped. Thus (A7) becomes

$$[K] \, \{u\} = \{F\}, \tag{A8}$$

where

$$K_{ij} = \iint_\Omega (\frac{\partial N_i}{\partial x} \frac{\partial N_j}{\partial x} + \frac{\partial N_i}{\partial y} \frac{\partial N_j}{\partial y})\ dxdy,$$

$$F_i = \iint_\Omega f\ N_i\ dxdy.$$

In this example, the Galerkin method was applied over the domain Ω. In the finite element method, the Galerkin method is applied by defining the approximation (A2) over small elements so that there is piecewise continuity within the domain. The contributions from each subdomain are summed to approximate the global domain.

Discretization of the Domain and Interpolation Functions

The ways of discretizing the domain are only limited by the imagination. In general, the governing equations or Galerkin integrals determine the minimum order of the approximation. Higher order approximation than that required may be used and in some cases may give better results. The geometry of the domain often determines the shape of the elements and placement of the nodes. Fig. Al shows a domain subdivided by the finite difference method. Fig. A2 shows how the same domain could be discretized for application of the finite element method. Note that in Fig. Al, there are several grid points outside the domain which require special handling. For the finite element discretization, Fig. A2, two elements were used. The domain shown could represent
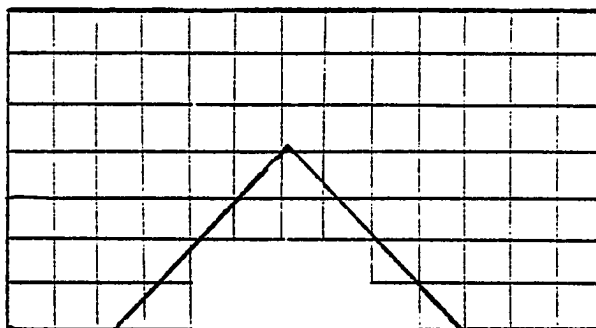
Fig. Al. Discretization of domain for finite differences.

flow in a channel with an obstruction. Fig. A2 shows some of
the flexibility of the finite element method in that finer
resolution is used over the obstruction and coarser resolu-
tion on the edges. Obviously, there are many possibilities
for discretization depending on the problem and the domain.
Discretization of the domain leads to development of the in-
terpolation functions.

Fig. A2. Discretization of domain for finite element method.

Finite Element Interpolation Functions

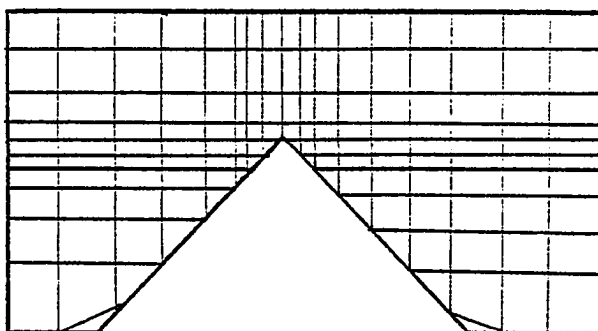There are two basic requirements for interpolation functions; completeness and compatibility. Suppose that the element equations contain derivatives of order m. The compatibility requirement means that at the interelement boundaries, the field variable and its partial derivatives up to order m-1 must be continuous. The completeness requirement means that within an element, all the constant states of the field variable and its derivatives up to order m must be represented in the interpolation function. That is, the polynomial used as the interpolation function must contain all the terms up to order m.

Suppose we have a system of equations in which first order derivatives are the highest order appearing in the Galerkin expressions. The compatibility requirement means that the minimum order for the interpolation functions is one. Assume that the global domain can be discretized using triangular shapes. We can choose the linear approximation

$$u(x,y) = a_0 + a_1 x + a_2 y. \qquad (A9)$$

Note that if a node is placed at each vertex of the triangle there are three unknowns (a_0, a_1, and a_2) corresponding to the three nodes. This polynomial satisfies the compatibility and completeness requirements. The next step is to determine the coefficients a_0, a_1, and a_2 for the arbitrary element
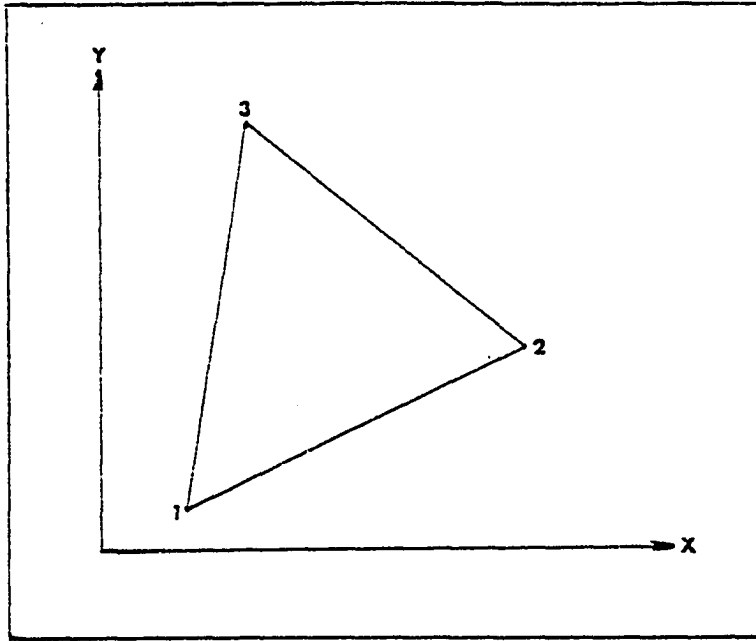
Fig. A3. Typical triangular element.

shown in Fig. A3.

From (A9) we get

$$
\begin{Bmatrix} u_1 \\ u_2 \\ u_3 \end{Bmatrix} = \begin{bmatrix} 1 & x_1 & y_1 \\ 1 & x_2 & y_2 \\ 1 & x_3 & y_3 \end{bmatrix} \begin{Bmatrix} a_0 \\ a_1 \\ a_2 \end{Bmatrix} \quad , \qquad \text{(A10)}
$$

or $\{u\} = [A]\ \{\alpha\}$,

$\{\alpha\} = [A]^{-1}\ \{u\}$,

where $[A]^{-1} = \dfrac{1}{\det} \begin{bmatrix} r_1 & r_2 & r_3 \\ s_1 & s_2 & s_3 \\ t_1 & t_2 & t_3 \end{bmatrix}$.

The determinant (det) of [A] turns out to be two times the area of the element. At any point (x,y) in the element

104

$$u = \{1 \ x \ y\} \ \{\alpha\} = \{1 \ x \ y\} \ [A]^{-1} \ \{u\} \ , \qquad \text{(A11)}$$

or
$$u = \sum_i N_i u_i,$$

where
$$N_i = \frac{1}{\det} (r_i + s_i \ x + t_i \ y).$$

$$r_i = x_j y_k - x_k y_j,$$
$$s_i = y_j - y_k, \qquad\qquad i \neq j \neq k$$
$$t_i = x_k - y_j.$$

Other Methods of Determining Interpolation Functions

There are several different means of deriving inter-polation polynomials. The most common method for rectangular shaped elements is to multiply the one dimensional polynomial for each dimension. That is, in one dimension we have

$$u(x) = b_0 + b_1 x \quad \text{or} \quad u(y) = b_2 + b_3 y.$$

If u were a function of x and y we would take the product

$$u(x,y) = a_0 + a_1 x + a_2 y + a_3 xy.$$

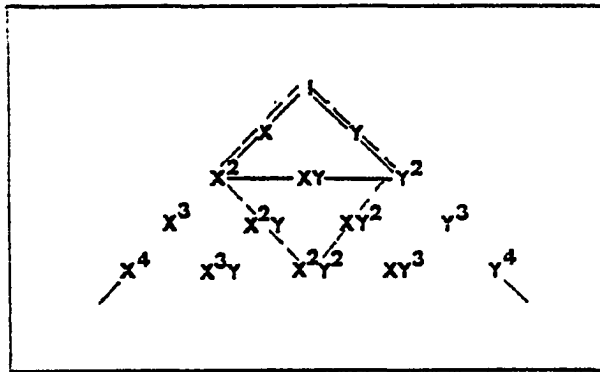Another method involves the use of Pascal's triangle [24].

Fig. A4. Pascal's Triangle

105

The terms connected by the solid line represent the terms
needed for a quadratic polynomial to be used on a triangular
element. There are six terms and such an element would have
six nodes. Note that the dashed line encloses nine terms.
these nine terms would be used for a nine-node rectangular
element. The location of the terms relative to the dashed
box indicated the nodal locations in the rectangle.

Local Coordinates

Previously the element was defined in terms of
the global coordinates (x,y); however, it is often conven-
ient to define the element in some local coordinate system
and later transform that system to the global coordinates.
This is especially true of the triangular element where an
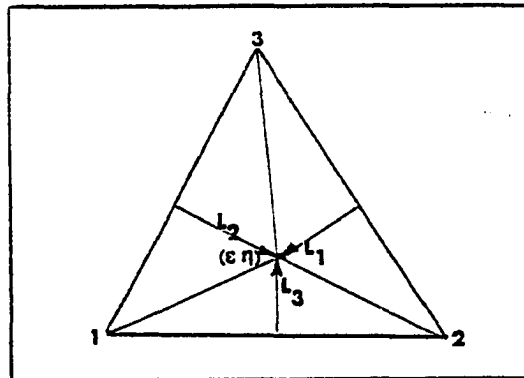area coordinate (Segerlind 1976) is convenient (see Fig. A5).
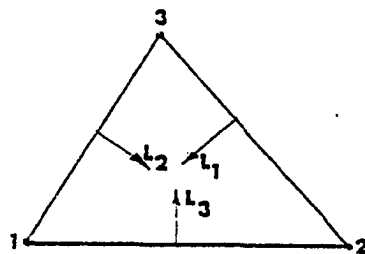

Fig. A5. Area coordinates for the triangle

The point (ε, η) in Fig. A5 divides the triangle into three areas (L_1, L_2, L_3). We can define the shape functions in terms of these areas. Let L be the total area of the element, then

$$N_i = L_i/L \qquad i = 1\text{-}3$$

$$L_1 + L_2 + L_3 = L$$

Interpolation Functions for the Elements Studied
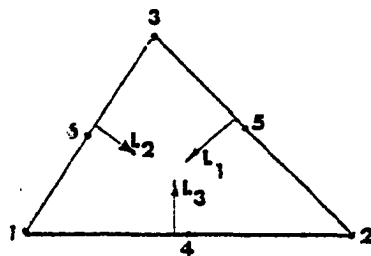
Linear Triangle

$$N_1 = L_1/L$$
$$N_2 = L_2/L$$
$$N_3 = L_3/L$$

Quadratic Triangle

$$N_1 = L_1/L(2L_1/L-1)$$
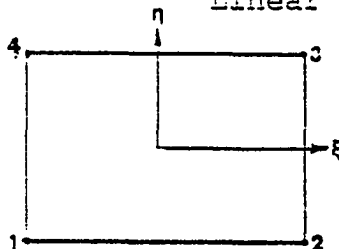$$N_2 = L_2/L(2L_2/L-1)$$
$$N_3 = L_3/L(2L_3/L-1)$$
$$N_4 = 4L_1L_2/L^2$$
$$N_5 = 4L_2L_3/L^2$$
$$N_6 = 4L_1L_3/L^2$$

Linear Rectangle

$$N_i = \frac{1}{4}(1+\xi\xi_i)(1+\eta\eta_i)$$

$$i = 1\text{-}4$$

Quadratic Rectangle (Lagrangian)
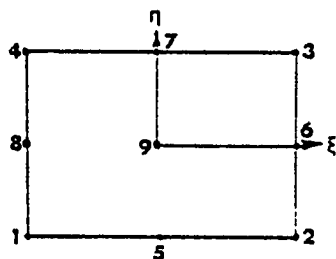
$$N_1 = \frac{1}{4}\,\xi\eta(1-\xi)(1-\eta)$$

$$N_2 = -\frac{1}{4}\xi\eta(1+\xi)(1-\eta)$$

$$N_3 = \frac{1}{4}\,\xi(1+\xi)\,\eta(1+\eta)$$

$$N_4 = -\frac{1}{4}\xi(1-\xi)\,\eta(1+\eta)$$

$$N_5 = -\frac{1}{2}\,(1-\xi^2)\eta(1-\eta)$$

$$N_6 = \frac{1}{2}\xi(1+\xi)(1-\eta^2)$$

$$N_7 = \frac{1}{2}\,(1-\xi^2)\,\eta(1+\eta)$$

$$N_8 = -\frac{1}{2}\xi(1-\xi)(1-\eta^2)$$

$$N_9 = (1-\xi^2)(1-\eta^2)$$

Quadratic Rectangle (Serendipity)
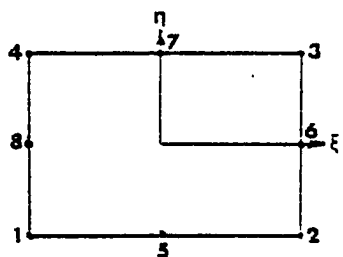
Corner Nodes: $i = 1-4$

$$N_i = \frac{1}{4}(1+\xi\xi_i)(1+\eta\eta_i)(\xi\xi_i+\eta\eta_i-1)$$

Mid-side Nodes:

$$\xi_i = 0 \quad N_i = \frac{1}{2}(1-\xi^2)(1+\eta\eta_i) \quad i = 5,7$$

$$\eta_i = 0 \quad N_i = \frac{1}{2}(1+\xi\xi_i)(1-\eta^2) \quad i = 6,8$$

APPENDIX B

LINEAR STABILITY ANALYSIS

Introduction

The purpose of this appendix is to show the linear stability analysis for the time differencing schemes used in this report. Because of the superior results achieved through the use of the four- node linear element, the stability analyses are only performed for that element. The technique used is the von Neuman method as discussed by Mesinger and Arakawa (1976).

Stability Analysis

Consider the linear advection equation,

$$\frac{\partial \phi}{\partial t} = - u_o \frac{\partial \phi}{\partial x} - v_o \frac{\partial \phi}{\partial y} , \qquad (B1)$$

where u_o and v_o are positive constants. This equation describes the advection of the variable ϕ at a constant velocity c given by,

$$c = (u_o^2 + v_o^2)^{\frac{1}{2}} \qquad (B2)$$

The variable ϕ is assumed to be of the form,

$$\phi(x,y,t) = \Phi(t) \exp[i(kx + ly)], \qquad (B3)$$

where k and l are wave numbers in the x and y directions, respectively.

The finite element method, using the four-node bi-linear element is applied to (B1) as discussed in Chapter III and Appendix A. By expanding the matrices in the resulting expression a finite difference form of the finite element equation is obtained. The resulting expression is

$$\frac{1}{36}[16\dot{\phi}(j,m) + 4(\dot{\phi}(j+1,m)+\dot{\phi}(j-1,m)+\dot{\phi}(j,m+1) +\dot{\phi}(j,m-1))$$

$$+ \dot{\phi}(j+1,m+1) +\dot{\phi}(j+1,m-1) +\dot{\phi}(j-1,m+1) +\dot{\phi}(j-1,m-1)]$$

$$= \frac{-u_o}{12\Delta x}[(\phi(j-1,m+1) -\phi(j-1,m-1)) + (\phi(j+1,m+1)-\phi(j+1,m-1)) \qquad (B4)$$

$$+4(\phi(j,m+1)-\phi(j,m-1))] \; \frac{-v_o}{12\Delta y} \; [(\phi(j+1,m-1)-\phi(j-1,m-1))$$

$$+(\phi(j+1,m+1)-\phi(j-1,m+1)) +4 (\phi(j+1,m) -\phi(j-1,m)],$$

where Δx and Δy are the grid spacing in x and y, respectively. This expression is valid at any interior grid point. The terms such as (j,m) indicate the grid point where $x = j\Delta x$ and $y = m\Delta y$.

Leap-frog

As discussed in Appendix A and Chapter III, the matrix form of (B4) is

$$[M] \ \{\dot{\phi}\}^{(n)} = - [K] \ \{\dot{\phi}\}^{(n)} \ , \qquad (B5)$$

where $[M]$ is the mass matrix and $[K] \ \{\phi\}^{(n)}$ represents the linear advection and the superscript indicates the time step. For the Leap-frog scheme, (B5) becomes

$$[M] \ \{\phi\}^{(n+1)} - [M] \ \{\phi\}^{(n-1)} = -2\Delta t [K] \ \{\phi\}^{(n)}. \qquad (B6)$$

Eq. (B3) is written in discrete form:

$$\phi^{(n)}(j,m) = \Phi_o \ \lambda^n \ \exp[i \ (kj\Delta x + lm\Delta y)], \qquad (B7)$$

where Φ_o is the initial amplitude and λ^n is the amplification factor to the nth power. Using the Eqs. (B4, B6, and B7) it can be shown that

$$\lambda^{n+1} \ \exp[i(kj\Delta x + lm\Delta y)] \ \frac{1}{9} \ (2 + \cos l\Delta y)(2 + \cos k\Delta x)$$

$$-\lambda^{n-1} \ \exp[i(kj\Delta x + lm\Delta y)] \ \frac{1}{9} \ (2 + \cos l\Delta y)(2 + \cos k\Delta x)$$

$$\qquad (B8)$$

$$= - \frac{\sqrt{2}}{6} \ i \ \lambda^n \ \exp[i(kj\Delta x + lm\Delta y)] \ \{\frac{u_o}{\Delta x} \ [\sin l\Delta y(2 + \cos k\Delta x)]$$

$$+ \frac{v_o}{\Delta y} \ [\sin k\Delta x(2 + \cos l\Delta y)]\} \ .$$

For simplification, assume that $u_o = v_o$ and $\Delta x = \Delta y = d$. Substituting (B2) into (B8) and simplifying gives

$$\lambda^2 + 3\sqrt{2} \ \frac{c\Delta t}{d} \ i\lambda \ (\frac{\sin ld}{2 + \cos ld} + \frac{\sin kd}{2 + \cos kd}) - 1 = 0. \qquad (B9)$$

The term in parenthesis in (B9) has a maximum value of $2/\sqrt{3}$. Making that substitution and solving for λ gives

$$\lambda = -\sqrt{6} \ \frac{c\Delta t}{d} \ i \pm (-6 \ \frac{c^2\Delta t^2}{d^2} + 1)^{\frac{1}{2}} \ . \qquad (B10)$$

It can easily be seen that

$$|\lambda| = 1 \qquad \text{if } \sqrt{6} \ \frac{c\Delta t}{d} \leq 1. \qquad (B11)$$

Therefore, the coupling of the time derivative through the consistent mass matrix as in (B4) results in a more restrictive time step than is found in finite difference applications or with lumped mass. A similar analysis is performed by Cullen (1974a).

If the left side of (B4) is replaced by the single term $\phi(j,m)$ then the stability criteria is

$$\sqrt{2} \ \frac{c\Delta t}{d} \leq 1. \qquad (B12)$$

"Theta-family" of Time Approximations

For the "theta-family" of time approximations discussed in Chapter III, (B5) becomes

$$[M]\{\phi\}^{(n+1)} - [M]\{\phi\}^{(n)} = -\theta\Delta t \ [K]\{\phi\}^{(n+1)} - (1-\theta)\Delta t [K]\{\phi\}^{(n)}. \qquad (B13)$$

Using Eqs. (B4, B7, and B13) as well as all the simplifications used to obtain (B10) gives

$$\lambda = \frac{1 - (1-\theta) \ pi}{1 + \theta pi} \ , \qquad (B14)$$

where $p = \sqrt{6} \ \frac{c\Delta t}{d}$.

For the Crank-Nicholson scheme, $\theta = 1/2$, and

$$|\lambda| = 1.$$

112

Therefore, the Crank-Nicholson scheme is always stable. For the Backward scheme, $\theta = 1$, and

$$|\lambda| = \frac{1}{1+p} \, .$$

If $p \geq 0$, this scheme is always stable but the solution is damped. The larger p is, the larger the damping effect. For the Galerkin scheme, $\theta = 2/3$, and

$$|\lambda| = \frac{1 + p/3}{1 + 2p/3} \, .$$

This scheme is also stable under the same conditions as the Backward scheme. Damping is also present in the Galerkin scheme but the damping is less than in the Backward scheme. If the "theta-family" of approximations is analyzed for lumped mass, the only difference in the result is that $p = \sqrt{2} \, \frac{c \Delta t}{d}$.